Uncertainty and Predictability of Tropical Cyclone Rainfall Based on Ensemble Simulations of Typhoon Sinlaku (2008)

CHUN-CHIEH WU, SHIN-GAN CHEN, SHIH-CHIEH LIN, TZU-HSIUNG YEN, AND TING-CHEN CHEN

Department of Atmospheric Sciences, National Taiwan University, Taipei, Taiwan

(Manuscript received 26 September 2012, in final form 13 April 2013)

ABSTRACT

Using special data from the field campaign of 2008 and an ensemble Kalman filter–based vortex initialization method, this study explores the impact of different track clusters categorized under the ensemble simulations of Typhoon Sinlaku (2008) on the associated precipitation. In particular, the distinct pattern of cumulative frequencies in the 28 members is identified to correspond to three types of track clusters. The simulation integrated from the initial ensemble mean slightly underestimates the maximum amount of the observed rainfall in central Taiwan by about 30%. The quantitative evaluation based on the equitable threat score indicates that members with tracks close to the best track produce more consistent rainfall distribution in northern Taiwan although their cumulative frequencies are underestimated. For members with southwestward-biased tracks, although the cumulative frequencies are closer to the observation, the simulated rainfall pattern is less consistent with the observation in northern Taiwan and the maximum rainfall amount is overestimated. The comparison of rainfall simulation during landfall between two representative members shows that the distinct differences in the rainfall amount and distribution are primarily associated with the track differences on the windward side of the mountain. With a finer horizontal grid resolution, the rainfall accumulation becomes greater as a result of the enhancement of updraft from the better-resolved topography, yet the cumulative frequency stays nearly unchanged. Based on ensemble simulations, this study highlights that the uncertainties in rainfall patterns and amounts can be assessed from ensemble track variations, thus providing better insights into the rainfall predictability associated with typhoons near Taiwan.

1. Introduction

The track forecasts of tropical cyclones (TCs) have been significantly improved over the past decades as a result of improved numerical weather models, advanced data assimilation schemes, and the increased amounts of satellite observations (Wu et al. 2007; Chou et al. 2011; Weissmann et al. 2011; Franklin 2012). However, besides TC intensity forecasts (Wang and Wu 2004), quantitative precipitation forecasting remains one of the most challenging and difficult tasks for operational prediction centers, such as the prediction of total rainfall amounts and rainfall distribution during the passage of TCs. The heavy rainfall associated with TCs often leads to devastating mudslides and floods, resulting in enormous economic loss and potential threats to human life. Therefore, research efforts to better understand the basic precipitation mechanism are very important for improving the TC precipitation prediction and to help mitigate damages and casualties.

Based on analyses from a series of historical heavy rainfall events, Lin et al. (2001) proposed several synoptic-scale and mesoscale conditions that are conducive to heavy orographic rainfall, such as a very moist low-level jet, steep orography, slow movement of the convective system, and a conditionally or potentially unstable upward airflow. The effect of Taiwan's topography on the track, intensity change, and precipitation distribution in Typhoon Herb (1996) was examined using a high-resolution mesoscale model (Wu et al. 2002). They showed that the resolution of horizontal grids and terrain plays an important role in capturing the mesoscale rainfall distribution. Consistent results were obtained in Yang et al. (2008), which showed that the decreased terrain height produces reduced accumulated rainfall in the simulation of Typhoon Nari (2001).

There are high uncertainties in the rainfall simulation associated with TCs in numerical models since the precipitation amount is affected by multiple factors, such as

Corresponding author address: Dr. Chun-Chieh Wu, Dept. of Atmospheric Sciences, National Taiwan University, No. 1, Sec. 4, Roosevelt Rd., Taipei 106, Taiwan.
E-mail: cwu@typhoon.as.ntu.edu.tw

DOI: 10.1175/MWR-D-12-00282.1

the track variation, the complicated interaction between the TC circulation and topography, and the detailed cloud microphysics (Wu and Kuo 1999). The ensemble forecast that uses multiple models or the increased numbers of ensemble member has been demonstrated to reduce forecast errors in terms of the 500-hPa geopotential height (Buizza and Palmer 1998) and the TC track (Goerss 2000). Accordingly, the ensemble forecast, which has been extensively applied in TC forecasts in recent years (Rappaport et al. 2009), can assist in understanding the uncertainties in rainfall simulation associated with TCs. Zhang et al. (2010) showed that the improved synoptic analysis field can be obtained by using a convection-permitting mesoscale ensemble data assimilation system, which better captures the extreme rainfall during Typhoon Morakot (2009). In addition, the impact of the storm translation speed on the rainfall simulation of Typhoon Morakot has been quantitatively explored based on the ensemble Kalman filter (EnKF) (Wu et al. 2010) in the Weather Research and Forecasting Model (WRF) (Yen et al. 2011). Their results showed that the 55% increase of the storm translation speed (36% reduction in the total time during Morakot's passage over Taiwan) leads to a 33% reduction in the maximum accumulated rainfall in southern Taiwan.

The implementation of vortex initialization in numerical models can effectively improve TC track forecasts (Wu et al. 2006; Chou and Wu 2008; Wu et al. 2010). Various ways had been designed to conduct vortex initialization, such as vortex bogusing and bogus data assimilation (Kurihara et al. 1995; Zou and Xiao 2000; Pu and Braun 2001; Wu et al. 2006). The abundant and valuable data collected during The Observing System Research and Predictability Experiment (THORPEX)–Pacific Asian Regional Campaign (T-PARC; Elsberry and Harr 2008) provide a unique opportunity to improve the initial environmental and TC vortex condition in the model. In particular, a new method that assimilates three special observation operators (i.e., the TC center position, storm motion vector, and axisymmetric surface wind profile) based on EnKF (Meng and Zhang 2007) was proposed in Wu et al. (2010) and used in this study to acquire a better and more balanced initial vortex in Typhoon Sinlaku (2008) during the T-PARC period. The ensemble simulation with the initial condition improved by the EnKF data assimilation can generate more insightful results than the deterministic run, especially with respect to the probabilistic rainfall forecast (Wu 2013). In addition, a series of research topics related to the targeted observations (Wu et al. 2012a), the structure change and concentric eyewall formation (Wu et al. 2012b; Huang et al. 2012), and the air–sea interaction (Sung et al. 2010) for Typhoon Sinlaku have been explored. This study focuses on the rainfall simulation for Typhoon Sinlaku, particularly on the relationship between rainfall distribution and track uncertainty. The description of model configuration, experimental design, and EnKF data assimilation scheme are given in section 2. Section 3 presents the simulation results, including the track, intensity, rainfall distribution, and the comparison between the control run and sensitivity experiments. A summary of this study is provided in section 4.

2. Methodology and experimental design

The EnKF method first proposed by Evensen (1994) is a powerful tool to optimally estimate model states from the background and observations with the flow-dependent background error statistics. It has been extensively adopted in atmospheric numerical models for the use of research in various topics (Snyder and Zhang 2003; Torn and Hakim 2009; Meng and Zhang 2007; Aksoy et al. 2009, 2010; Zhang et al. 2009) as well as for operational weather prediction systems (Szunyogh et al. 2008; Torn and Hakim 2008; Whitaker et al. 2008; Aksoy et al. 2013). Wu et al. (2010) applied the ensemble square root filter (Whitaker and Hamill 2002) to assimilate three newly proposed observation operators for TCs. This same WRF-based EnKF data assimilation system is adopted in this study.

The Advanced Research WRF (ARW) (version 3.2.1) is used to perform update cycle ensemble simulations. The horizontal resolution is 45 km (81 × 76 grid points), 15 km (88 × 100 grid points), and 5 km (160 × 151 grid points) in the first (D1), second (D2), and third (D3) fixed domains, respectively (Fig. 1). Thirty-five vertical levels are used in the terrain-following sigma coordinate. The physics parameterization schemes include the WRF single-moment 6-class microphysics scheme (WSM6; Hong et al. 2004; Hong and Lim 2006), the Rapid Radiative Transfer Model (RRTM) scheme (Mlawer et al. 1997) for longwave radiation, the simple shortwave scheme (Dudhia 1989) for shortwave radiation, and the Yonsei University (YSU) planetary boundary layer scheme (Hong et al. 2006). The cumulus convection is parameterized with the Grell–Dévényi ensemble scheme (Grell and Dévényi 2002) only in the coarser domains, namely, D1 and D2.

Taking the National Centers for Environmental Prediction (NCEP) Final Analysis (FNL; 1° × 1°) at 1200 UTC 8 September 2008 as the initial condition, the 28 ensemble members are generated by randomly perturbing the mean analysis in a transformed streamfunction field as described in Zhang et al. (2006). After the prerun in the first 5 h, the cycling assimilation run is carried out

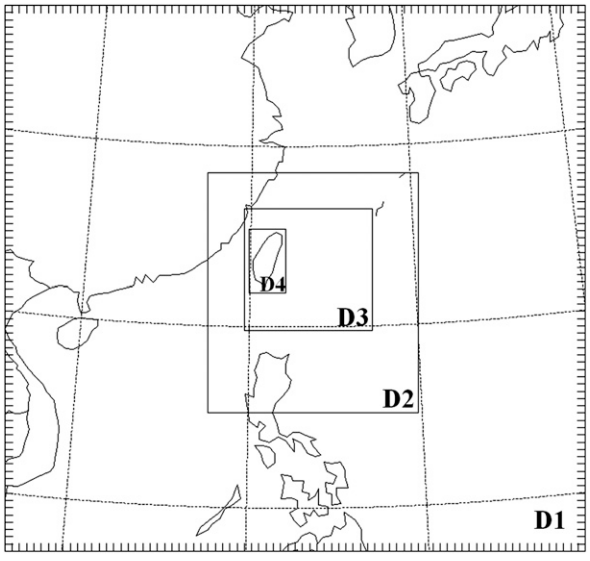

FIG. 1. Four domains of WRF. The innermost domain with a 1.67-km horizontal resolution (D4) is used only in the sensitivity experiment.

from 1700 UTC 8 September to 1200 UTC 11 September 2008 by using the method as in Wu et al. (2010). The conventional radiosondes, dropwindsondes obtained during T-PARC, satellite observations, and three special observation operators (the same as those indicated in the introduction) are assimilated into the model with an update cycle of every 30 min.

The 4-day ensemble simulation with 28 members initialized at 1200 UTC 11 September 2008 for Typhoon Sinlaku (after the cycling EnKF data assimilation had been performed) is regarded as the control experiment (CTL). In addition, the simulation that is integrated from the initial condition derived from the ensemble mean (the average of 28 members) is conducted and denoted as CTL-M. The difference between CTL-M simulation and the ensemble mean could be expected as a result of the effect of nonlinear integration. Meanwhile, in order to examine the effect of model resolution and to better resolve the terrain-induced precipitation, another experiment using the additional fourth domain with a 1.67-km horizontal resolution (D4) near Taiwan (Fig. 1) is carried out. The D4 domain only employs one-way feedback from its parent domain (D3). Figure 2 shows the actual topography of Taiwan and model topographies in D3 and D4 of WRF and indicates the counties in which the mountains are located, following the discussions in this paper. As expected, the model topography resolved in D3 (Fig. 2b) is much rougher than that in D4 (Fig. 2c), which appears similar to the actual topography (Fig. 2a).

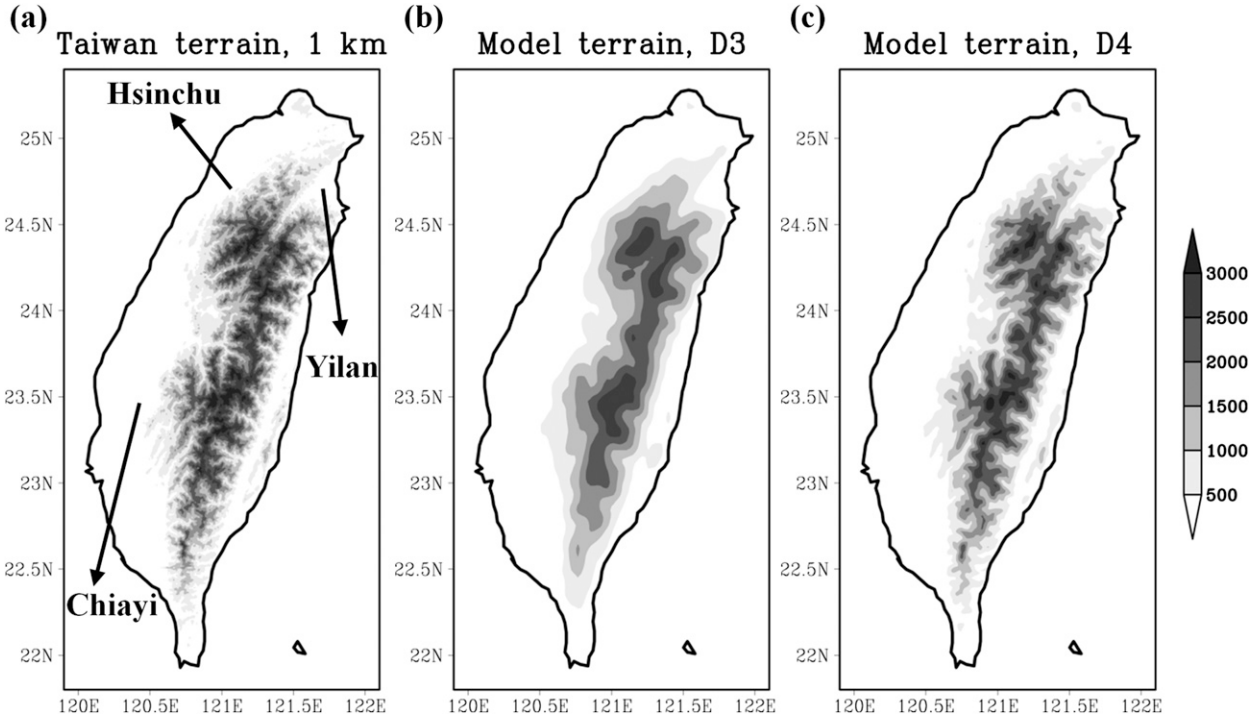

FIG. 2. Terrain height (m) of Taiwan (a) from observation data with 1-km resolution; and used in WRF in (b) D3 with 5-km resolution and (c) D4 with 1.67-km resolution.

To quantitatively evaluate how different ensemble members perform in the rainfall simulation, the equitable threat score (ETS; Schaefer 1990; Black 1994; Chien et al. 2002; Marchok et al. 2007) is employed. Higher ETS indicates the model simulation is more capable of capturing the observed rainfall pattern at a certain rainfall threshold. In particular, two areas with heavy rainfall [one is northern Taiwan (NT) and the other is central Taiwan (CT), as indicated by the rectangular boxes in Fig. 4a] are chosen to calculate the ETS for the comparison of forecast performance among different members.

3. Results

Figure 3a shows the ensemble tracks of 28 members and CTL-M from 1200 UTC 11 September to 0000 UTC 15 September 2008. The track in CTL-M is generally consistent with the best track analyzed by the Central Weather Bureau (CWB) of Taiwan although its translation speed is slightly higher than that of the best track at later forecast times. The track forecast errors are 62, 47, and 95 km at 24, 48, and 72 h, respectively (Table 1). Note that the track errors at these three forecast times are smaller than the mean CWB official forecast errors of about 85, 133, and 211 km, respectively, for this case (Lu 2008), indicating that the simulation through the EnKF data assimilation can well capture the observed track of Sinlaku. However, the ensemble tracks among 28 members show a large spread (Fig. 3a), indicating there are high uncertainties associated with the initial conditions and model errors.

The minimum sea level pressure (MSLP) in CTL-M at the initial time is about 950 hPa, which is higher than the best-track estimations from CWB and Japan Meteorological Agency (JMA) by about 25 and 15 hPa, respectively (Fig. 3b). It rises slightly and remains at around 955 hPa until 1200 UTC 13 September 2008. Later the storm begins to weaken after landfall (the landfall time in CTL-M is at 0000 UTC 14 September and the observed landfall time is at 1800 UTC 13 September 2008). At around 1500 UTC 12 September 2008, the storm intensity in CTL-M is close to the observation measured by C-130 reconnaissance flight although it is weaker than the CWB and JMA estimations by about 10 to 30 hPa. Note that the sea level pressure from C-130 reconnaissance is derived by the flight-level geopotential height, which is more accurate than that estimated from satellites (Martin 1988; Naval Research Laboratory 1999). The tendency of intensity change in 28 ensemble members is generally consistent with that in CTL-M. In addition, the MSLP averaged by 28 members is nearly identical to that in the CTL-M simulation, indicating that the integration from the initial condition of ensemble mean is able to reasonably identify the mean intensity tendency among all members. Nevertheless, the initial MSLP has a weak bias in the ensemble simulations and the rate of the weakening during the landfall period is slightly slower than observed. Thus, the model cannot precisely capture the intensity evolution both at initial and forecast times, likely due to the vortex spinup after data assimilation and the limitation of model resolution.

The 3-day accumulated rainfall in Taiwan from 0000 UTC 12 September to 0000 UTC 15 September 2008 observed by using rain gauges and the CTL-M simulation in D3 are shown in Figs. 4a,b. Although there are multiple local maxima in the observed accumulated rainfall (Fig. 4a), three distinct regions with extreme rainfall amounts in the Central Mountain Range (CMR) of Taiwan can be identified: the southwestern slope near Chiayi (about 1109 mm), the northwestern slope near Hsinchu (about 1211 mm), and the northeastern slope near Yilan (about 1195 mm). The simulation in CTL-M only marginally captures the distribution of the rainfall maxima while a number of rainfall maxima in the observation are missing (Figs. 4a,b). Quantitatively, the extreme rainfall amounts over the mountains near Hsinchu and Chiayi are underestimated in the CTL-M run, but those over the mountain near Yilan are slightly overestimated. The accumulated rainfall of 749 mm over the southwestern slope of CMR underestimates the observed rainfall amount by about 30%. One of the reasons for this underestimation is related to the limited model resolution (5 km) in the finest domain used in the simulation, which is likely insufficient for resolving the cloud microphysical process and the interaction between the storm and the terrain. In addition, the presence of the initial weak bias in the MSLP as shown in Fig. 3b could be another factor, and may in part explain why the simulations underpredict the total rainfall, despite not being the focus of this paper.

To understand the variation in the rainfall amounts among ensemble members, the cumulative frequency (Wu et al. 2002) of the total rainfall in D3 based on the data points over Taiwan is compared to the rain gauge observation (Fig. 4c). The cumulative frequency indicates the area percentage of the landmass in Taiwan above a certain rainfall amount. It is evident that the cumulative frequencies in 28 members fall into three groups with different distribution patterns (red, blue, and yellow lines in Fig. 4c). It can be found that these three groups correspond to three types of track clusters (Fig. 5): the southwest-biased group (SWB; Fig. 5a), the no-biased group (NOB; Fig. 5b), and the northeast-biased group (NEB; Fig. 5c) as compared to the best track. The track

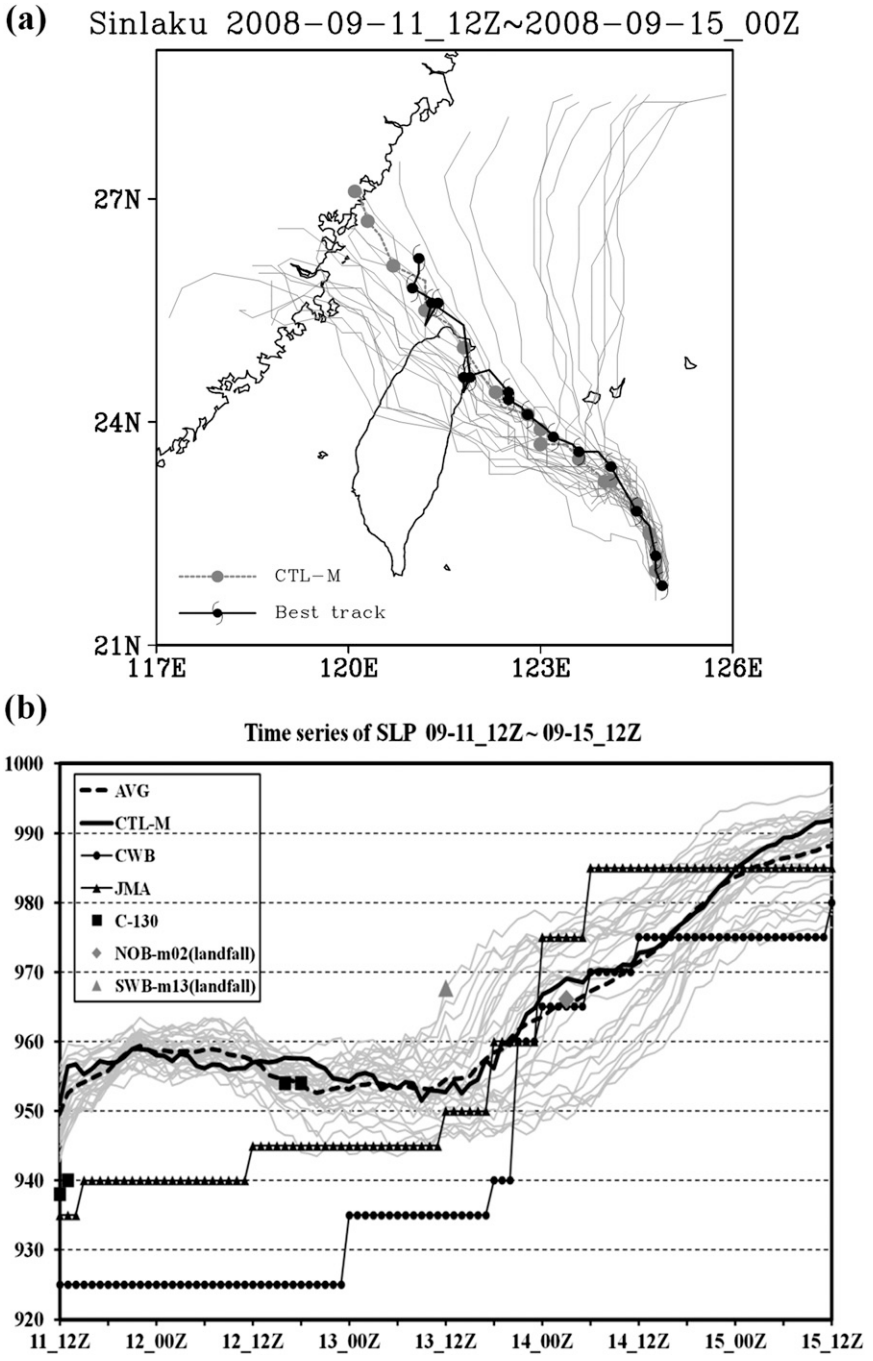

FIG. 3. (a) The best track of CWB (typhoon symbols), and the simulated tracks in CTL-M (closed circles) and 28 members (gray lines) from 1200 UTC 11 Sep to 0000 UTC 15 Sep 2008 for every 6 h. (b) Time evolution of the minimum central pressure (hPa) analyzed by CWB (line with closed circles) and JMA (line with triangles), and in CTL-M (solid black line), 28 ensemble members (gray lines), as well as their average value (dashed black line) from 1200 UTC 11 Sep to 1200 UTC 15 Sep 2008. The closed squares indicate the minimum sea level pressure measured from two C-130 reconnaissance flights during T-PARC. The gray diamond and triangle indicate the TC intensity at the landfall time in NOB-m02 and SWB-m13, respectively.

TABLE 1. Track forecast errors (km) verified by the best track of CWB from 12 to 72 h initialized at 1200 UTC 11 Sep 2008 in CTL-M, NOB-m02, SWB-m13 (the largest southward bias), and NEB-m24 (the largest northward bias).

Track errors	12 h	24 h	36 h	48 h	60 h	72 h
CTL-M	11	62	49	47	45	95
NOB-m02	35	64	40	47	11	55
SWB-m13	49	25	78	123	198	242
NEB-m24	16	89	121	212	357	437

for member 13 (24) has the largest southward (northward) bias with an error of 242 (437) km at 72 h (Table 1). In addition, the 12–72-h mean track forecast error of about 42 km for member 02 is the smallest (Table 1; Fig. 5b). Therefore, members 13, 02, and 24 are taken as the representative member of SWB, NOB, and NEB, respectively (hereafter denoted as SWB-m13, NOB-m02, and NEB-m24, respectively). In section 3a, the impact of different track clusters on the rainfall simulation is examined.

a. Effect of different track clusters on the rainfall

Figure 6 shows the 3-day accumulated rainfall from 0000 UTC 12 September to 0000 UTC 15 September 2008 in the ensemble mean of members in SWB, NOB, and NEB (as well as the representative member in each group). In SWB, local maximum rainfall amounts are located over the mountain area near Yilan and along the southwestern slope of CMR near Chiayi (Figs. 6a,b). The accumulated rainfall maximum near Yilan in SWB-m13 is about 2552 mm (1945 mm in the ensemble mean of SWB), which is much higher than the observed value of 1195 mm. On the contrary, the simulated rainfall amount over the mountain area near Chiayi (about 1000 mm) is slightly lower than the observation (1109 mm). Because of the southwestward track bias, the windward location (upslope of the mountain) induced by TC circulation would shift to the south, thus leading to the different rainfall pattern and amount as compared to the observation.

In NOB, the maximum accumulated rainfall over the mountain area near Chiayi is about 860 mm in NOB-m02 (697 mm in the ensemble mean of NOB; Figs. 6d,e), moderately lower than the observed value of 1109 mm. Figure 5c shows that the simulated storms in NEB turn to the north earlier than the best track, and that landfall does not occur in all members. Consequently, the simulations in both NEB-m24 and the ensemble mean of NEB are not able to accurately identify the distribution and amount of accumulated rainfall (Figs. 6g,h) as compared to the observation. The accumulated rainfall amount in northern Taiwan does not exceed 700 mm and the precipitation is quite limited in central and southern regions of Taiwan. SWB has the largest standard deviation of accumulated rainfall in northeastern Taiwan (Fig. 6c), indicating that the variability of rainfall simulation among members in SWB is larger than that among members in NOB and NEB.

As mentioned above, the criterion for categorizing the members into three groups is based on the cumulative frequency of the total rainfall. Taking 500 mm as an example, the area with accumulated rainfall amount higher than this threshold accounts for about 30% of the total area in SWB, 15% in NOB, and 5% in NEB (Fig. 4c). In SWB, the simulated tracks and rainfall distribution (Figs. 5a and 6a,b) are much different from the observation although the cumulative frequencies are closer to the observed curve than those of the other two groups in cases of rainfall amounts ranging between 100 and 500 mm (Fig. 4c). It is likely that the overestimation of the accumulated rainfall in SWB associated with the southwestward track bias in part compensates for the underestimation caused by the insufficient model resolution, thus leading to the coincidental agreement of cumulative frequency between SWB and the observation. Nevertheless, it should be noted that the cumulative frequency of the total rainfall simply indicates the percentage of areas with rainfall amount exceeding a certain threshold, and thus it cannot actually reflect the rainfall pattern and the location of maximum rainfall. In both NOB and NEB, the cumulative frequencies mostly lie beneath the observed curve. Even though the tracks are well simulated in NOB (Fig. 5b), the model is unable to accurately capture the percentage of areas with rainfall amounts exceeding 50 mm. In addition, the observed cumulative frequency is significantly underestimated by the simulation of NEB since most rainfall occurs in the open ocean area as simulated storms move northward away from Taiwan.

The quantitative evaluation of ETS calculated in NT and CT (as indicated in Fig. 4b) is shown in Fig. 7 to compare the capability in simulating rainfall distribution among the ensemble mean of three different groups as well as their representative members. The ETS based on 3-day accumulated rainfall in NT in NOB-m02 is the highest at almost all rainfall thresholds (except at thresholds of 200, 900, and 1000 mm; Fig. 7a). In addition, the ETS in NT in the ensemble mean of members in SWB is lower than that in CTL-M and the mean of NOB when the rainfall threshold is above 300 mm. On the contrary, in CT the ensemble mean of SWB generally outperforms CTL-M and the mean of the other two groups (Fig. 7b). Such a higher ETS is likely in part due to the southwestward track bias, which incidentally offsets the undersimulation of rainfall associated with

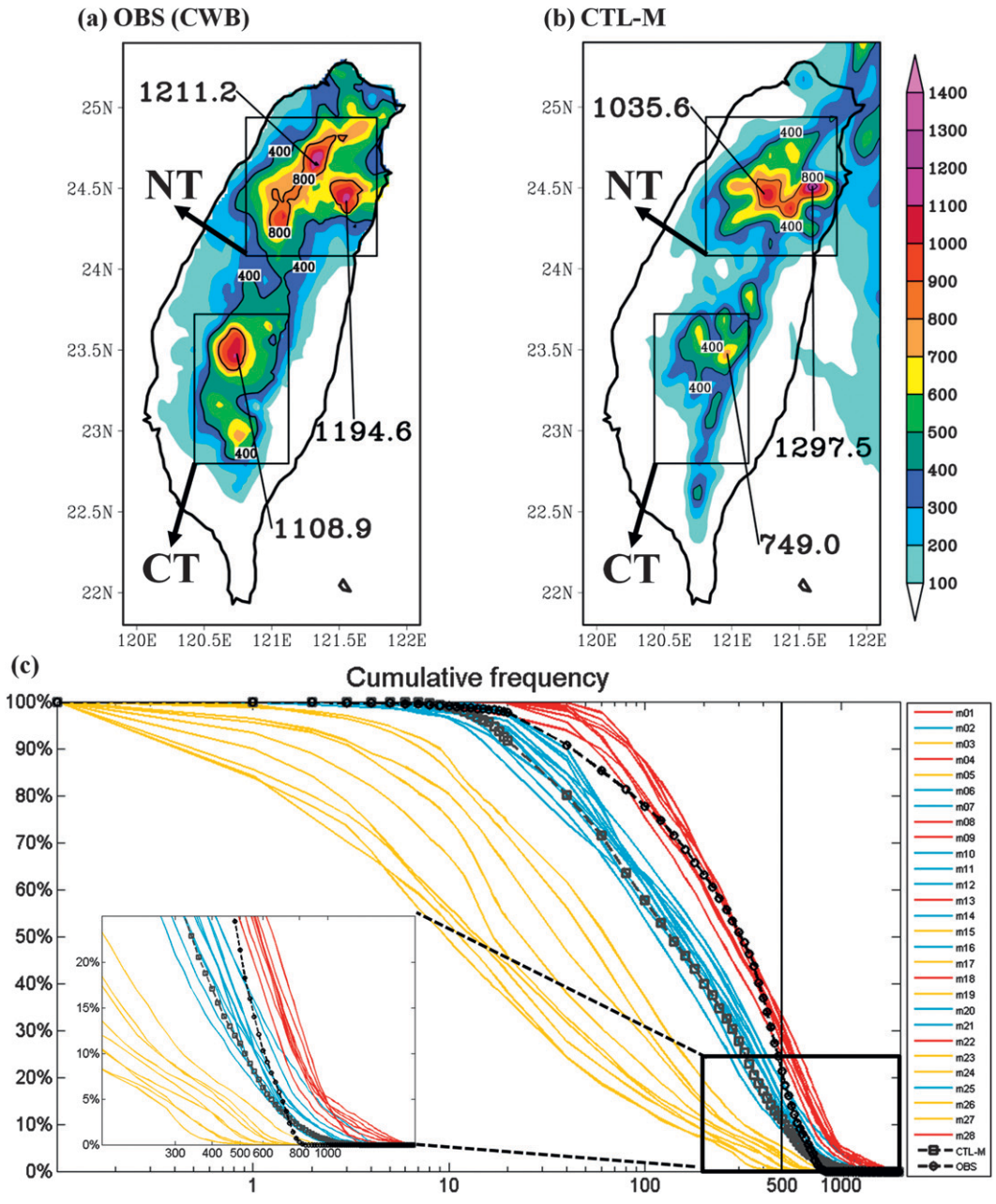

FIG. 4. The 3-day accumulated rainfall (mm) in D3 from 0000 UTC 12 Sep to 0000 UTC 15 Sep 2008 (a) in the observational data of CWB and (b) in CTL-M. The numbers indicate the local maximum. Two boxes denoted by NT and CT are the areas where the ETS is calculated. (c) The cumulative frequency of total rainfall from 0000 UTC 12 Sep to 0000 UTC 15 Sep 2008 in CTL-M (dashed line with squares), SWB (red lines), NOB (blue lines), NEB (yellow lines) based on the data points over the island of Taiwan, and the observation calculated from rain gauges in CWB (dashed line with circles). The abscissa is in the logarithmic scale of millimeter.

the limitation of model resolution. Since the simulations in CTL-M and the ensemble mean of NOB moderately underestimate the observed rainfall amount in CT (Figs. 4b and 6e), their associated ETS is below 0.1 at rainfall thresholds above 500 mm (Fig. 7b). As expected, the simulations in NEB have the lowest ETS in both NT and CT, with a value always below 0.1 at all rainfall thresholds. Meanwhile, the fact that the ETS in both NT and CT is almost always below 0.1 at rainfall thresholds above 800 mm in CTL-M and the ensemble mean of three groups (as well as their representative members) indicates the insufficient skills in identifying

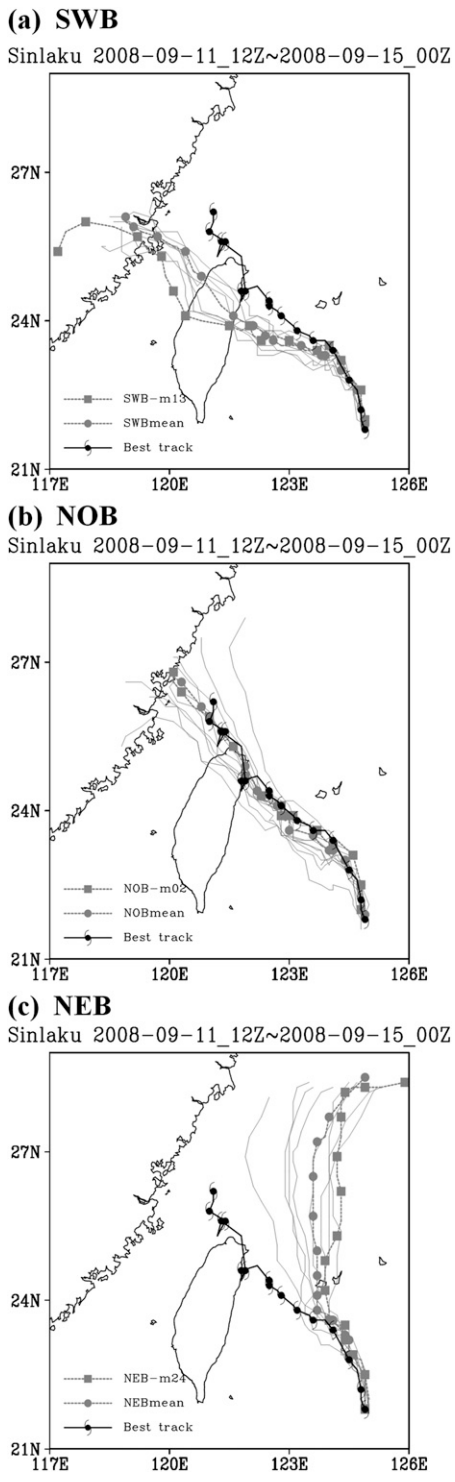

FIG. 5. The ensemble tracks in (a) SWB, (b) NOB, and (c) NEB from 1200 UTC 11 Sep to 0000 UTC 15 Sep 2008. The line with typhoon symbols indicates the best track of CWB. The lines with circles and squares indicate the track of ensemble mean and representative member in each group, respectively. The mark is plotted by the time interval of every 6 h.

the distribution of large rainfall amounts in these simulations. It is interesting to note that the ETS in both areas in CTL-M is almost identical to that in the ensemble mean of NOB at all rainfall thresholds, indicating that similar mean tracks would lead to similar rainfall patterns in the ensemble.

In all, the rainfall feature is distinctive in the three groups corresponding to the three different types of TC tracks. Consistent with Wu and Kuo (1999), this result highlights the role of track uncertainty in affecting the distribution and amount of accumulated rainfall.

b. Rainfall distribution during the landfall period

Since TCs in NEB do not make landfall in Taiwan (Fig. 5c), and because they produce a limited amount of accumulated rainfall (Figs. 6g,h), only simulations in SWB and NOB are examined, in order to focus on issues of major rainfalls in Taiwan. Instead of comparing the ensemble mean of SWB and NOB, the representative members in these two groups, SWB-m13 and NOB-m02, are demonstrated for comparison during the landfall period.

Since the landfall time in the simulation of each member is not always the same as the actual landfall time of the best track, it is not fair to compare the two groups based on the actual landfall time. We take the landfall time of each member as the base time (denoted as 0 h) for comparing the results of the two representative members and the observation. The time before and after landfall is indicated by the time with minus and positive signs, respectively. Figures 8a,b show the simulated track in NOB-m02 and SWB-m13 from 12 h before landfall (−12 h) to 12 h after landfall (+12 h), which is depicted by four 6-h time intervals. The 6-hourly averaged translation speed in four time intervals calculated by dividing the total distance of the storm movement by 6 h is shown in Fig. 8c. The translation speeds in NOB-m02 and SWB-m13 are close to each other in four time intervals, except for the time period from 0 to +6 h (Fig. 8c). The translation speed in NOB-m02 from approximately −6 to 0 h and from approximately 0 to +6 h is closer to that in the best track as compared to that in SWB-m13 while both speeds are larger (smaller) than the observation during approximately −12 to −6 h (approximately +6 to +12 h). The mean speeds from −12 to +12 h in NOB-m02 and SWB-m13 are 13.3 and 13.5 km h^{-1}, respectively, both of which are nearly the same as the best-track value of 13.2 km h^{-1}, indicating that the impact of translation speed on rainfall differences during the landfall period is limited in this case.

Figure 9 shows the accumulated rainfall in the observation, NOB-m02, and SWB-m13 during four 6-h time periods from −12 to +12 h. The observed accumulated

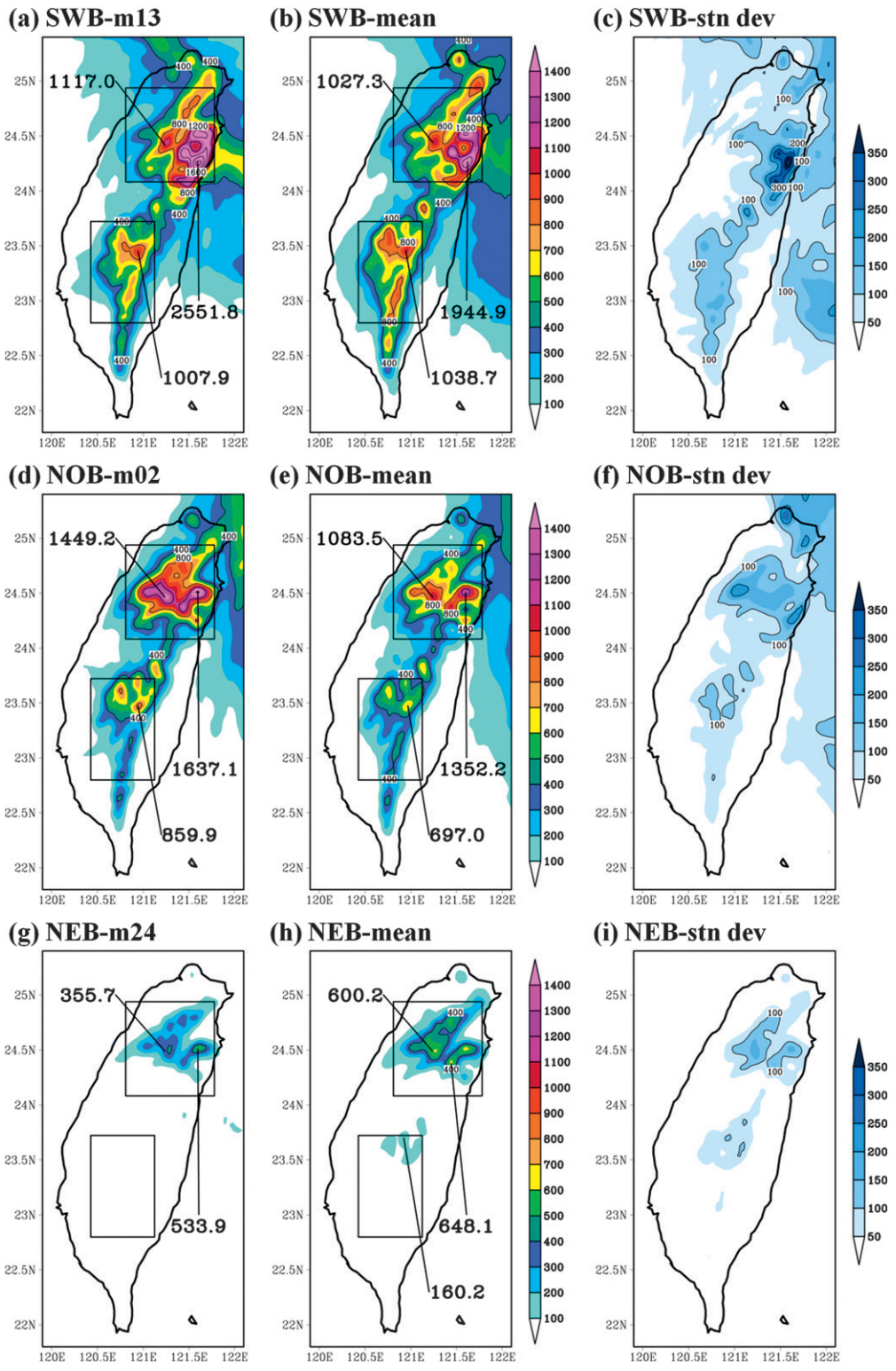

FIG. 6. The 3-day accumulated rainfall (mm) in D3 from 0000 UTC 12 Sep to 0000 UTC 15 Sep 2008 in (a) SWB-m13 and (b) the ensemble mean of members in SWB. (c) Standard deviation of the 3-day accumulated rainfall in SWB. (d)–(f) As in (a)–(c), but in NOB. (g)–(i) As in (a)–(c), but in NEB.

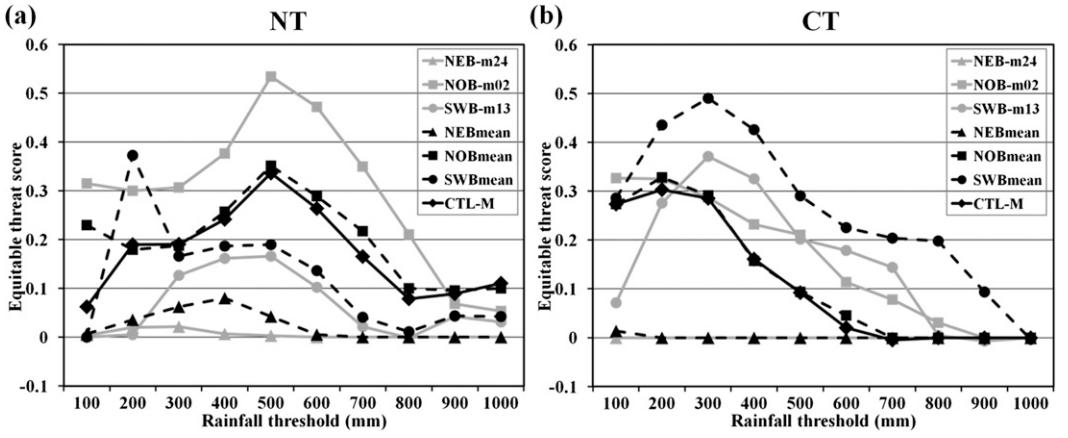

FIG. 7. The ETS of the 3-day accumulated rainfall forecasts from 0000 UTC 12 Sep to 0000 UTC 15 Sep 2008 calculated in (a) NT and (b) CT in CTL-M (black diamond), SWB-m13 (gray circle), NOB-m02 (gray square), NEB-m24 (gray triangle), and the ensemble mean of members in SWB (black circle), NOB (black square), and NEB (black triangle).

rainfall before landfall is mainly located in northern Taiwan, with the maximum value above 200 mm over the mountain area near Yilan (Figs. 9a,b). After Sinlaku's landfall, the location of the maximum rainfall is shifted to the mountain area near Hsinchu and the precipitation area in central Taiwan grows larger (Fig. 9c). The rainfall amount in central Taiwan increases during approximately from +6 to +12 h, with a local maximum value of about 235 mm (Fig. 9d). In the simulation in NOB-m02, the locations of two local rainfall peaks in northern Taiwan before landfall (Figs. 9e,f) do not well match the observation. Nevertheless, it is evident that the primary rainfall signal shifts from the mountain area near Yilan before landfall (Figs. 9e,f) to that near Hsinchu after landfall (Fig. 9g), and this is generally consistent with the observation although the simulated maximum rainfall is larger than the observed amount. On the contrary, in SWB-m13 the heavy rainfall signal from the prelandfall to postlandfall period remains over the mountain area near Yilan (Figs. 9i–l). Meanwhile, both the peak rainfall mount and the area with heavy rainfall are considerably overestimated in SWB-m13 during the landfall period. Regarding the rainfall forecast skills during the landfall period, the ETS based on the 6-h accumulated rainfall before landfall (approximately from −6 to 0 h) and after landfall (approximately from 0 to +6 h) is shown in Fig. 10. In NT, the ETS in NOB-m02 during the 6 h after landfall (approximately from 0 to +6 h) increases significantly at rainfall thresholds between 100 and 160 mm as compared to that before landfall (approximately from −6 to 0 h), while the ETS in SWB-m13 turns from positive values before landfall to negative values after landfall (Fig. 10a). In contrast, the difference of the ETS in CT prior to and after landfall for rainfall thresholds above 60 mm is relatively small in both NOB-m02 and SWB-m13 (Fig. 10b).

To understand the reason why the distribution of accumulated rainfall during landfall in Fig. 9 shows distinct difference between NOB-m02 and SWB-m13, the moisture and wind fields are examined. The 700-hPa relative humidity at 6 h before landfall in NOB-m02 is evidently low in southeastern Taiwan (leeward location and downslope of CMR; Fig. 11a), with the value below 50%. At 0 and +6 h, eastern Taiwan is still located to the lee side of the CMR and thus is drier than western Taiwan (Figs. 11d,g). The magnitude and area of dryness in southeastern Taiwan at −6 h in SWB-m13 are smaller (Fig. 11b) as compared to that in NOB-m02. In addition, in SWB-m13 northeastern Taiwan at landfall and after landfall (Figs. 11e,h) appears moister than that in NOB-m02 since it is located on the windward side (westward and northwestward wind associated with the storm circulation). In addition to factors associated with storm circulation, the rainfall distribution may also be modulated by the environmental features, such as the large-scale moisture field and the midlatitude trough (Atallah and Bosart 2003). To reduce the signal from the storm center displacement and to obtain the environmental field, the filtering method of Kurihara et al. (1993, 1995) is employed to remove the TC-scale component. The difference in 700-hPa relative humidity between NOB-m02 and SWB-m13 at the initial time after the TC component has been filtered out in D1 (the outermost domain) is smaller than 5% around the original locations of TC centers, as well as near the Taiwan area (figure not shown), indicating that the environmental moisture difference is relatively small in the analysis field. During the landfall period from −6 to +6 h, the difference in relative humidity is below 10% around the TC centers while a larger difference is shown at a distance from the centers (Figs. 11c,f,i). The relative

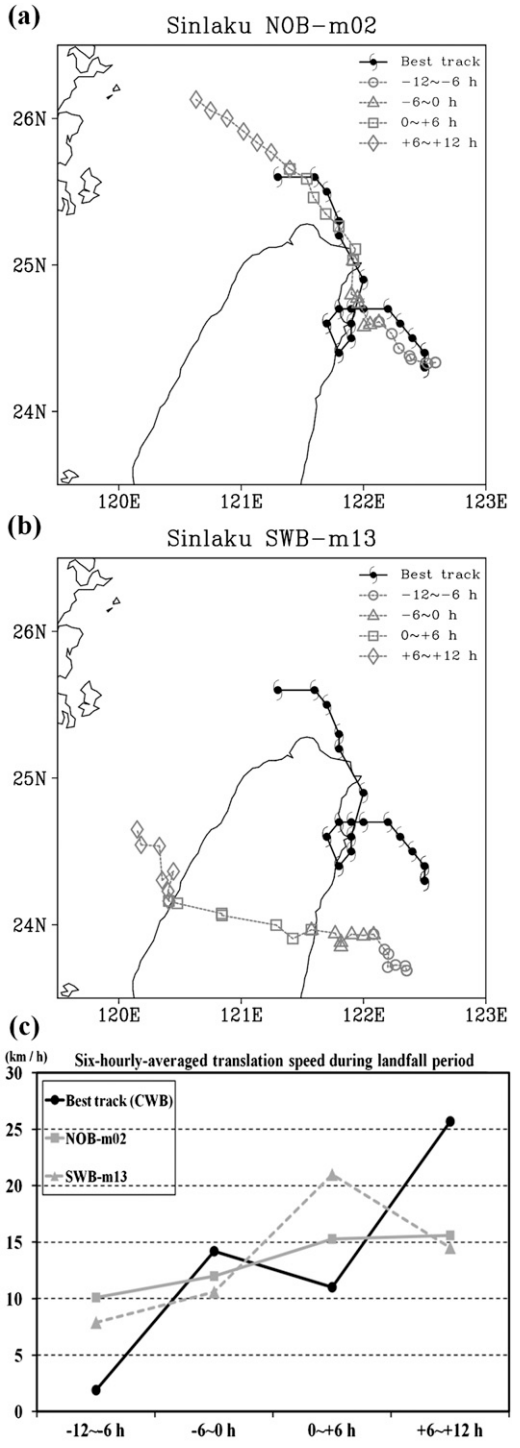

FIG. 8. The best track of CWB (typhoon symbol) and the simulated track in (a) NOB-m02, and (b) SWB-m13 during the period from 12 h before landfall to 12 h after landfall for every 1 h. The time before landfall, at landfall, and after landfall is denoted by the minus sign (−), zero (0), and the positive sign (+), respectively. The tracks in four time intervals of approximately from −12 to −6 h (circle), −6 to 0 h (triangle), 0 to +6 h (square), and +6 to +12 h (diamond) are shown. (c) 6-hourly averaged translation speed in four time intervals in the best track (circle), NOB-m02 (square), and SWB-m13 (triangle).

humidity difference is almost negative in the vicinity of Taiwan, indicating that the environmental humidity over Taiwan in NOB-m02 is slightly lower than that in SWB-m13 during the landfall period. Since this signal is very weak, the role of large-scale moisture differences in affecting the rainfall distribution differences appears insignificant. Meanwhile, although Corbosiero and Molinari (2002) and Rogers et al. (2003) had indicated the impact of vertical wind shear on the TC rainfall distribution, this issue is beyond the scope of this paper and would not be discussed here.

Because there are two main regions with heavy rainfall signal along around 23.5° and 24.5°N as indicated in Fig. 9 in both NOB-m02 and SWB-m13, the cross section of wind and relative humidity along these two latitudes is further studied. It is shown in Fig. 12a that the eastern slope of the mountain along 24.5°N is on the windward side before landfall. After landfall, the windward location is changed from the eastern slope to the western slope of the mountain (Figs. 12b,c) when the storm center in NOB-m02 moves farther north of 24.5°N (Figs. 11d,g). This change in the windward side could be one of the causes for the shift of maximum rainfall signal along 24.5°N from the eastern slope of the mountain before landfall (Figs. 9e,f) to the western slope after landfall (Fig. 9g). In contrast, the windward side along 23.5°N in NOB-m02 remains on the western slope of the mountain during the landfall period (Figs. 12d–f) and the relative humidity on the lee side of the mountain is evidently low as a result of the presence of a strong downdraft.

The simulated track in SWB-m13 during the landfall period is located between 23.5° and 24.5°N (Fig. 8b). Therefore, the eastern slope of the mountain along 24.5°N is always on the windward side from −6 to +6 h (Figs. 13a–c), which is different from the result of NOB-m02 showing the change in the windward location (Figs. 12a–c). Since the windward location along 24.5°N in SWB-m13 does not vary from the prelandfall period to postlandfall period, the heavy rainfall signal persistently occurs in northeastern Taiwan (Figs. 9j,k), which is not in accord with the observation (Figs. 9b,c). Consequently, this leads to a deterioration of the ETS in NT after landfall (Fig. 10a). Note that the wind speed on the eastern slope of the mountain along 24.5°N is quite large (Figs. 13b,c) and this can enhance the orographic lifting, thus leading to an overestimation of accumulated rainfall of about 553 mm in northeastern Taiwan during the 6-h period after landfall (Fig. 9k) as compared with the observation. Similar to NOB-m02, the windward region along 23.5°N in SWB-m13 occurs on the western slope of the mountain during the landfall period (Figs. 13d–f). Because the windward locations along 23.5°N in both NOB-m02 and SWB-m13 remain

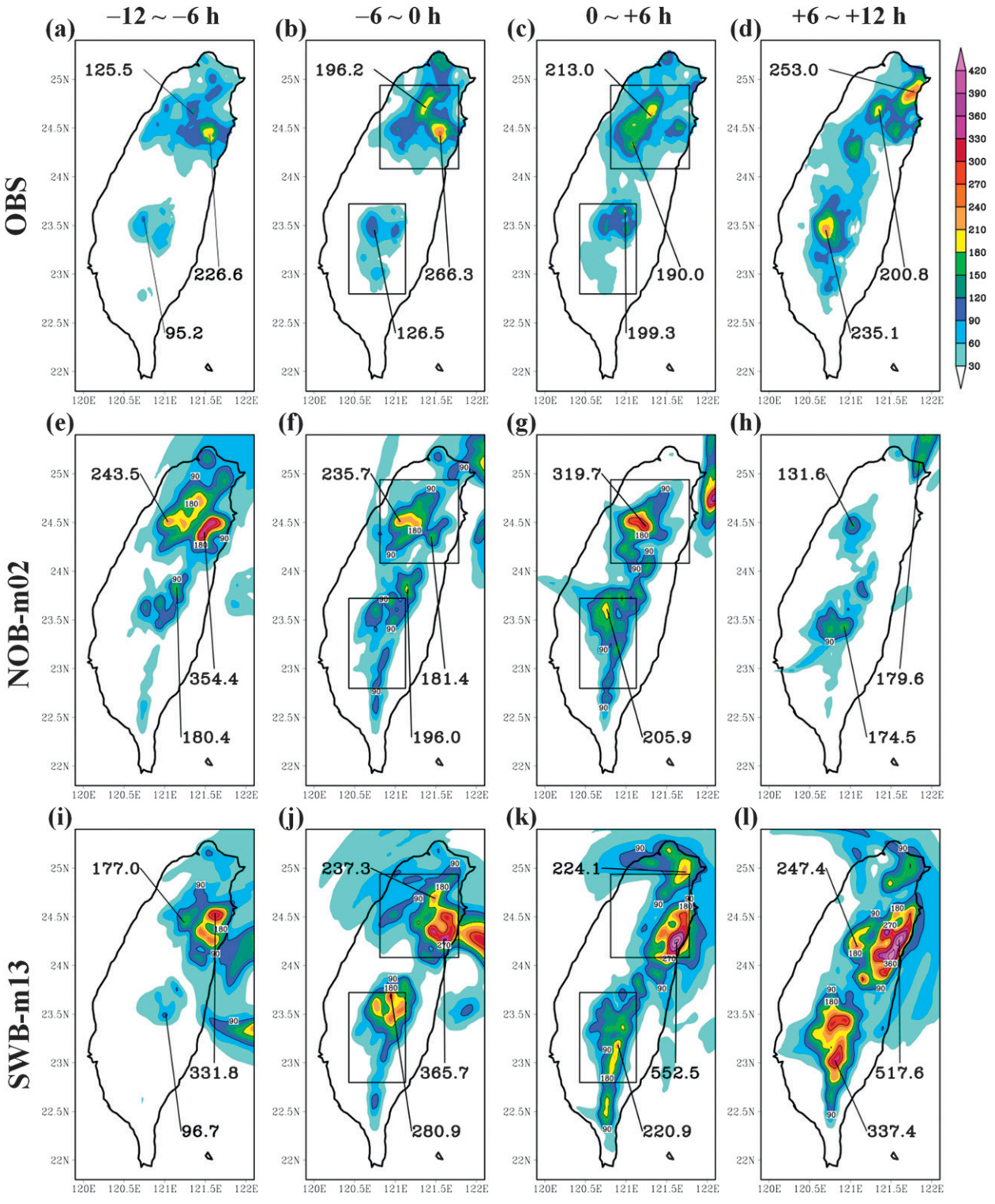

FIG. 9. The accumulated rainfall (mm) in the observational data of CWB during approximately (a) −12 to −6 h, (b) −6 to 0 h, (c) 0 to +6 h, and (d) +6 to +12 h. The landfall time is at around 1800 UTC 13 Sep 2008. (e)–(h) As in (a)–(d), but in NOB-m02 in D3. (i)–(l) As in (a)–(d), but in SWB-m13 in D3.

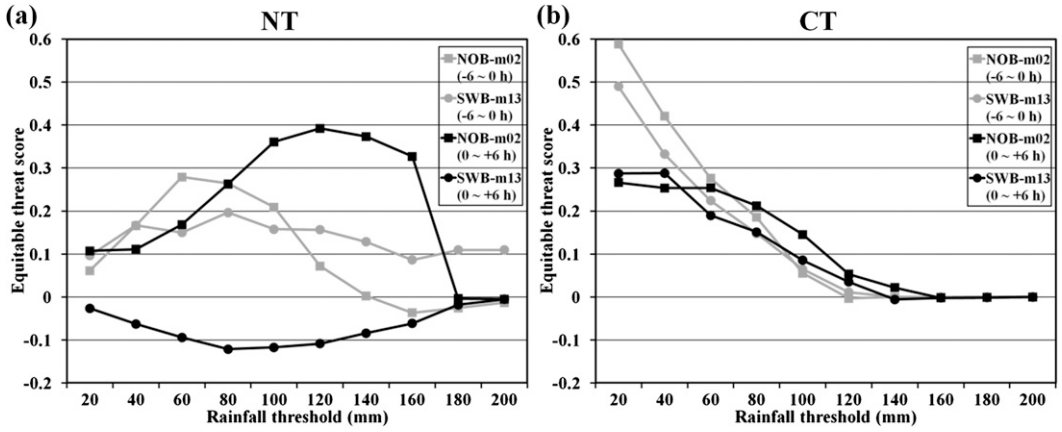

FIG. 10. The ETS of the 6-h accumulated rainfall forecasts during approximately from −6 to 0 h (gray) and from 0 to +6 h (black) calculated in (a) NT and (b) CT in NOB-m02 (square) and SWB-m13 (circle).

the same, the overall rainfall pattern is similar between prelandfall and postlandfall periods, thus leading to the limited variation of ETS in CT in both simulations (Fig. 10b).

The TC intensity and size, which may in part be influenced by different tracks, could be another factor affecting the rainfall amount and distribution. Thus, a comparison is made for the intensity and structure of storms between NOB-m02 and SWB-m13. The minimum central pressures in NOB-m02 and SWB-m13 are close to each other at the time of landfall, both of which are slightly higher than the value in the best track of CWB and JMA (the observed landfall is at around 1800 UTC 13 September) by about 8 hPa (Fig. 3b). In addition, the azimuthal mean storm structure in NOB-m02 at 1 h from the initial time and during the 24 h before landfall (Figs. 14a,b) is similar to that in SWB-m13 (Figs. 14d,e). It is indicated that the difference in intensity and structure of storms between NOB-m02 and SWB-m13 is small prior to landfall. Nevertheless, the azimuthal mean structure in NOB-m02 is evidently different from that in SWB-m13 during the landfall period (Figs. 14c,f). In SWB-m13, the maximum tangential wind and inflow are located outside the radius of about 120 km away from the center (Fig. 14f), which is nearly twice as large as the radius in NOB-m02 (Fig. 14c). Meanwhile, the magnitudes of both the maximum tangential wind and inflow in SWB-m13 are smaller than those in NOB-m02. Similar results are obtained in the ensemble mean of NOB and SWB (figure not shown). As compared to the structure in NOB-m02, the storm in SWB-m13 becomes weaker during landfall, likely experiencing more dissipation over the land surface due to the southward track bias. The fact that SWB-m13 produces larger rainfall amount than NOB-m02 suggests that the role of storm intensity and structure in affecting the rainfall simulation is secondary. In summary, the difference of simulated tracks between NOB-m02 and SWB-m13 results in the variation of windward locations during the landfall period, which in turn influences the rainfall distribution.

c. Sensitivity to the model resolution

To examine whether the underestimation of 3-day accumulated rainfall in central Taiwan in the simulations (e.g., Figs. 4b, 6a, and 6d) is associated with the insufficient horizontal resolution in the model (5 km), another sensitivity experiment using the fourth nested domain with the finest resolution of 1.67 km (D4; Fig. 1) is conducted. Figure 15 shows the 3-day accumulated rainfall in D4 in CTL-M, NOB-m02, and SWB-m13 as well as their corresponding cumulative frequencies in both D3 and D4. The comparison of results using 1.67-km resolution with those using 5-km resolution indicates that the maximum accumulated rainfall in central Taiwan increases as the horizontal resolution increases (cf. Figs. 15a,b,c and 4b, 6d, 6a, respectively) although the higher-resolution simulation turns out to overpredict the observation in northern and northeastern Taiwan. The maximum rainfall amount in central Taiwan in CTL-M increases from 749 (Fig. 4b) to 1033 mm (Fig. 15a) in the higher-resolution simulation, which is very close to the observed value of 1109 mm (Fig. 4a). It should be noted that even though the horizontal resolution is improved to 1.67 km, the model is still unable to precisely identify the peak rainfall amount (mostly with an overestimation in northern Taiwan). This result suggests the limitation of heavy rainfall simulation, partly related to the interaction of the storm, terrain, and model physics (such as cloud microphysics; Wu and Kuo 1999; Zhu and Zhang 2006; Tao et al. 2011). There is not much difference between

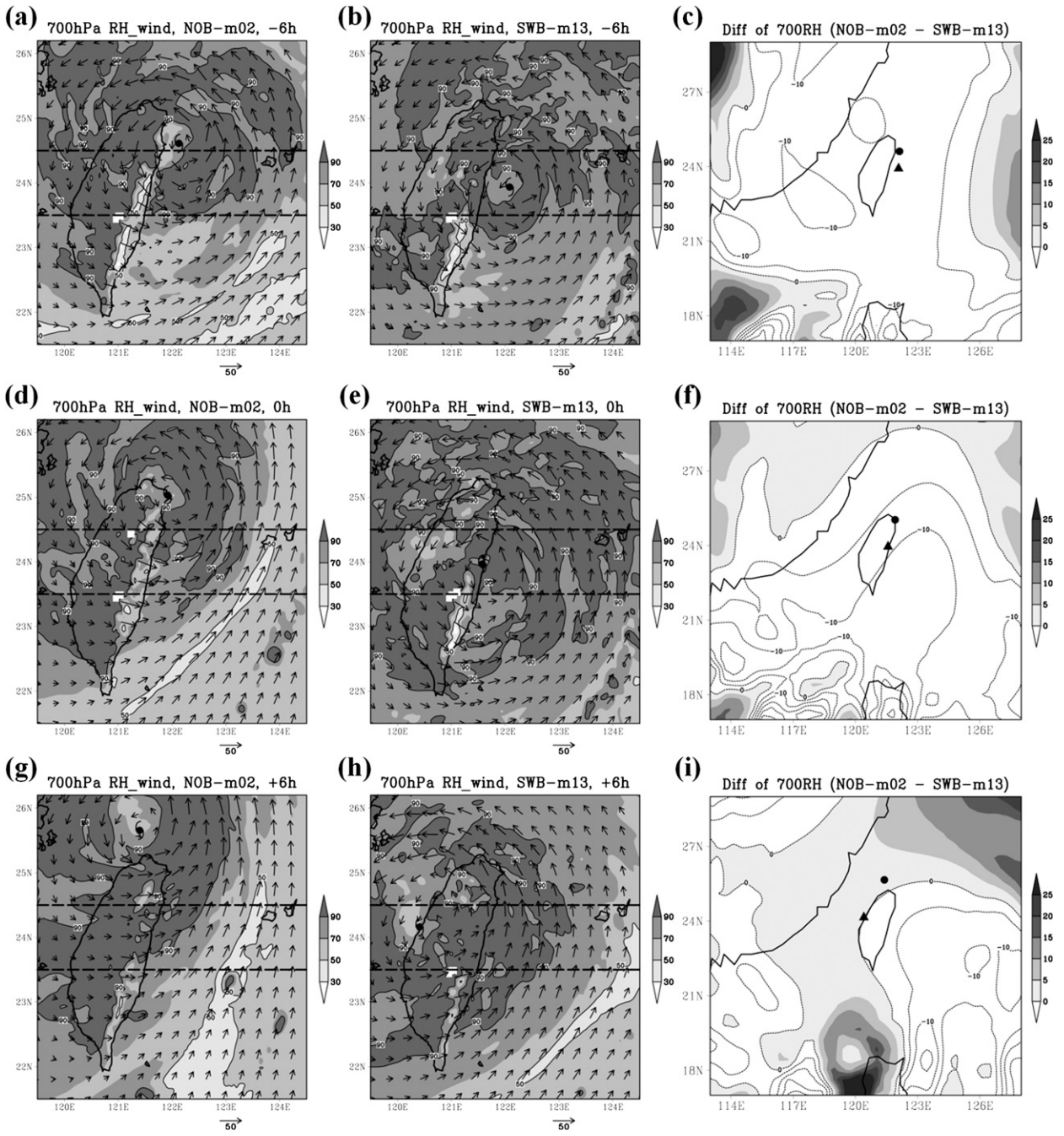

FIG. 11. The 700-hPa horizontal wind (arrow; m s^{-1}) and relative humidity (shading; %) in D3 at 6 h before landfall (−6 h) in (a) NOB-m02 and (b) SWB-m13. Two horizontal dashed lines indicate latitudes (24.5° and 23.5°N) for plotting the cross section in Figs. 12 and 13. (c) The difference of 700-hPa relative humidity between NOB-m02 and SWB-m13 with TC components filtered out in D1 at −6 h. Positive values are shaded and negative values are plotted by dashed contours with intervals of 5%. The solid circle and triangle indicate TC center positions of NOB-m02 and SWB-m13, respectively. (d)–(f) As in (a)–(c), but at the landfall time (0 h). (g)–(i) As in (a)–(c), but at 6 h after landfall (+6 h).

the curves calculated in D3 and D4 (Fig. 15d), indicating that the cumulative frequency is not sensitive to model resolution. In other words, increasing the grid resolution has limited influence on the percentage of areas with accumulated rainfall amount of a certain level, although the maximum accumulated rainfall is increased at some locations. In NT, the ETS calculated in D4 does not increase significantly as compared to that in D3 (figure

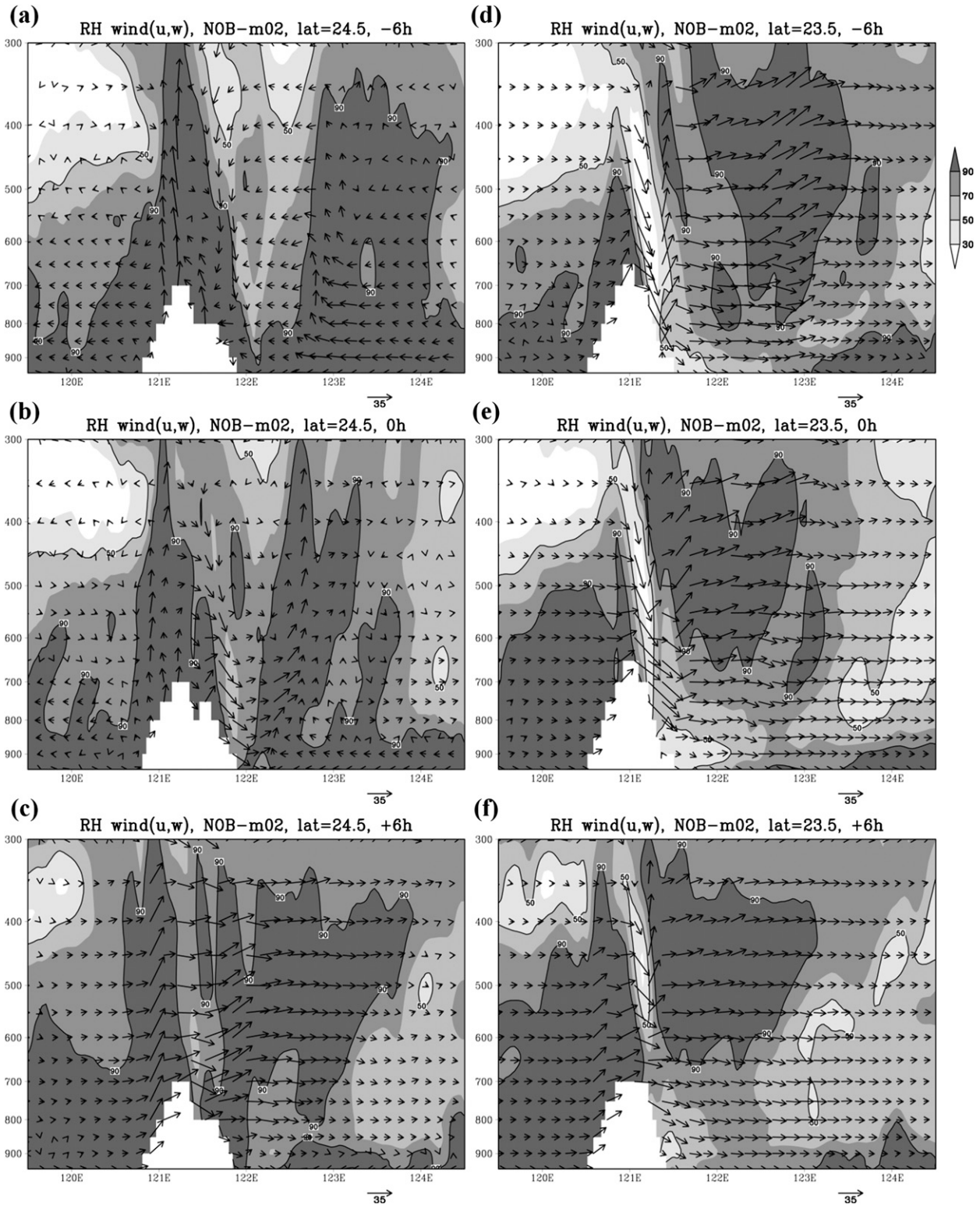

FIG. 12. The cross section of wind (u, w; vertical wind is multiplied by 10 m s^{-1}) and relative humidity (shading; %) along 24.5°N (indicated in Fig. 11) in NOB-m02 (a) at 6 h before landfall (−6 h), (b) at the landfall time (0 h), and (c) at 6 h after landfall (+6 h). (d)–(f) As in (a)–(c), but along 23.5°N (indicated in Fig. 11). The vertical pressure coordinate is in logarithmic scale.

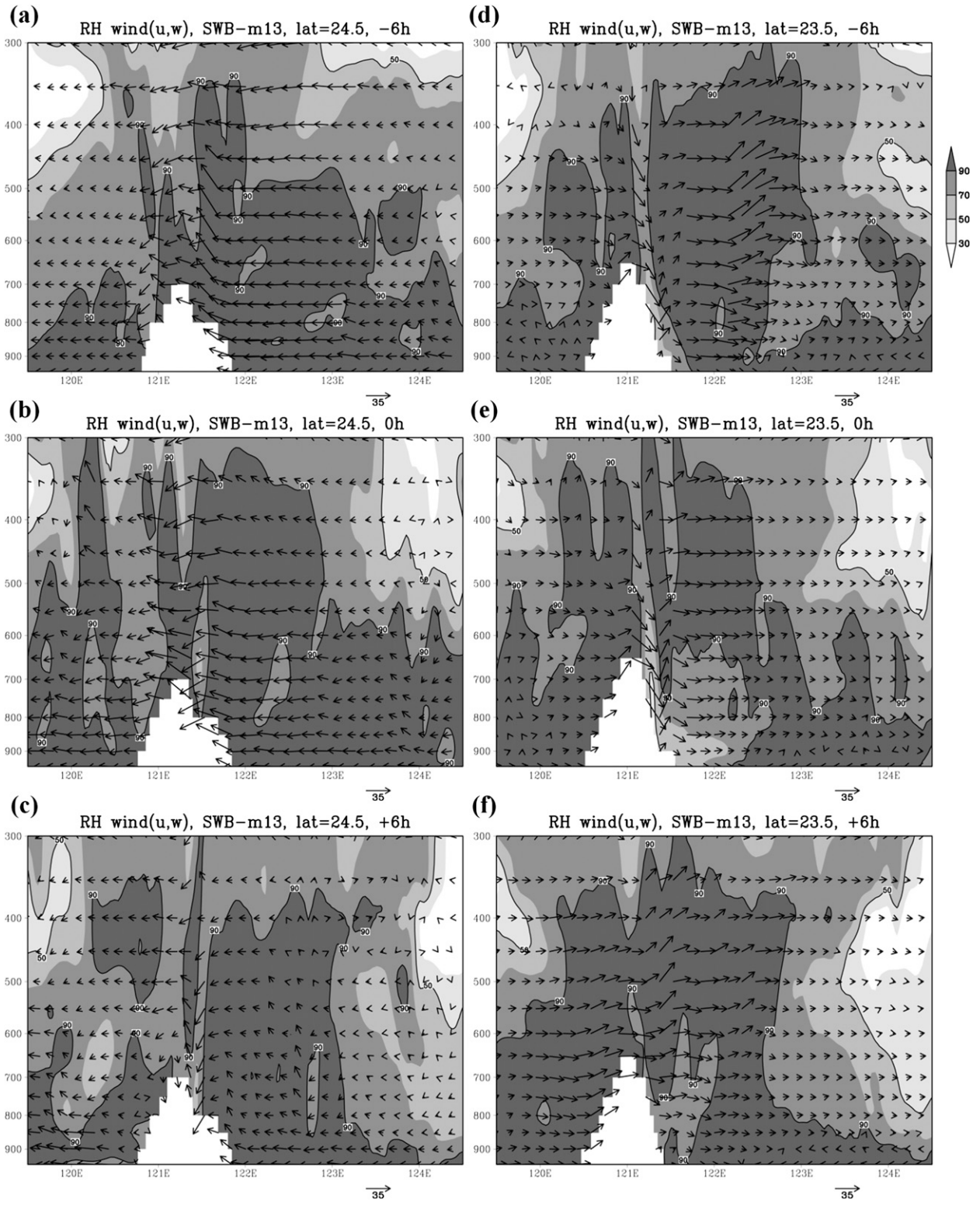

FIG. 13. As in Fig. 12, but in SWB-m13.

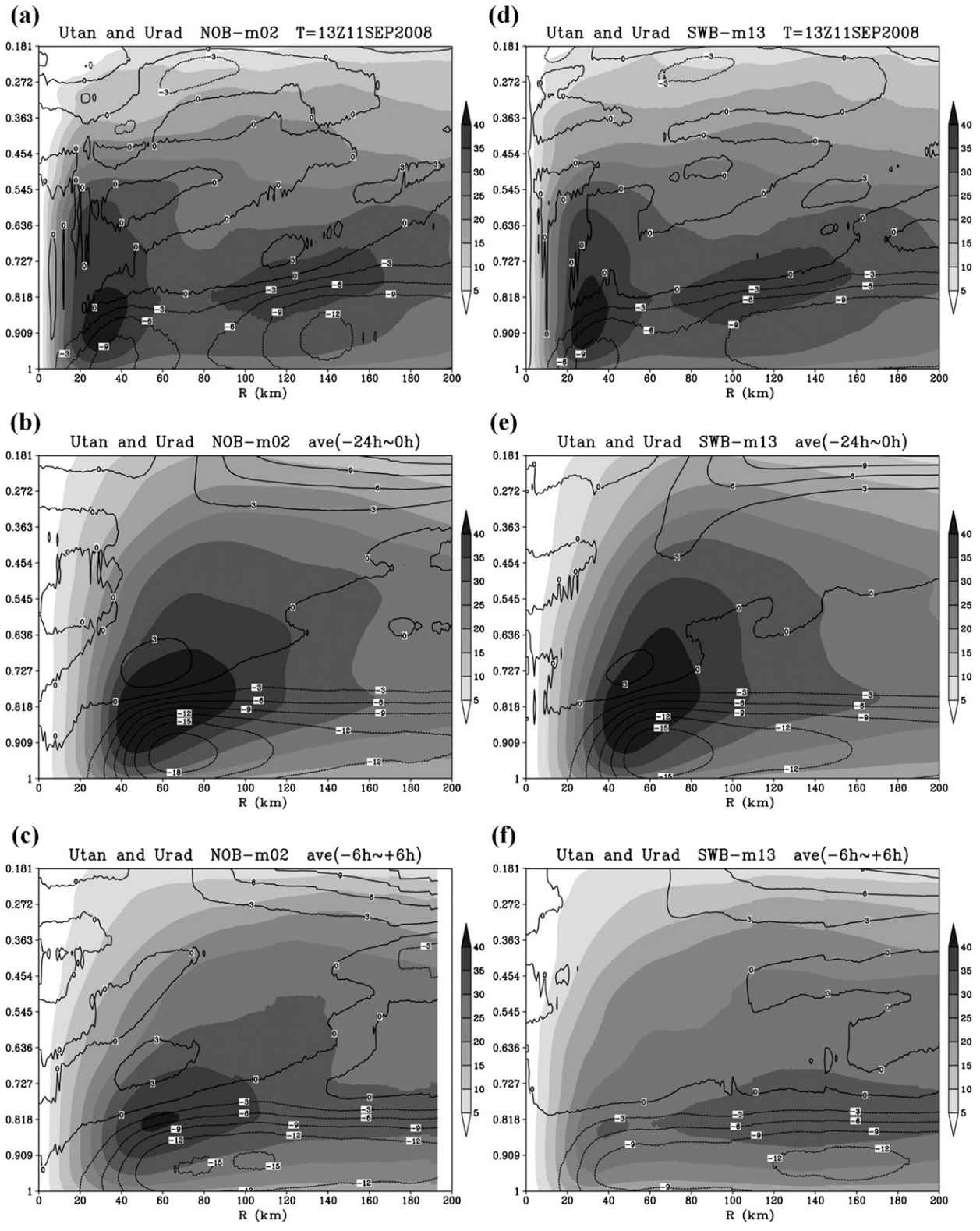

FIG. 14. The azimuthal mean structure of tangential wind (shading; m s^{-1}) and radial wind (contours with intervals of 3 m s^{-1}) in NOB-m02 (a) at 1 h from the initial time, (b) averaged from 24 h before landfall to the time of landfall, and (c) averaged from 6 h before landfall to 6 h after landfall. The vertical coordinate is at sigma levels. (d)–(f) As in (a)–(c), but in SWB-m13.

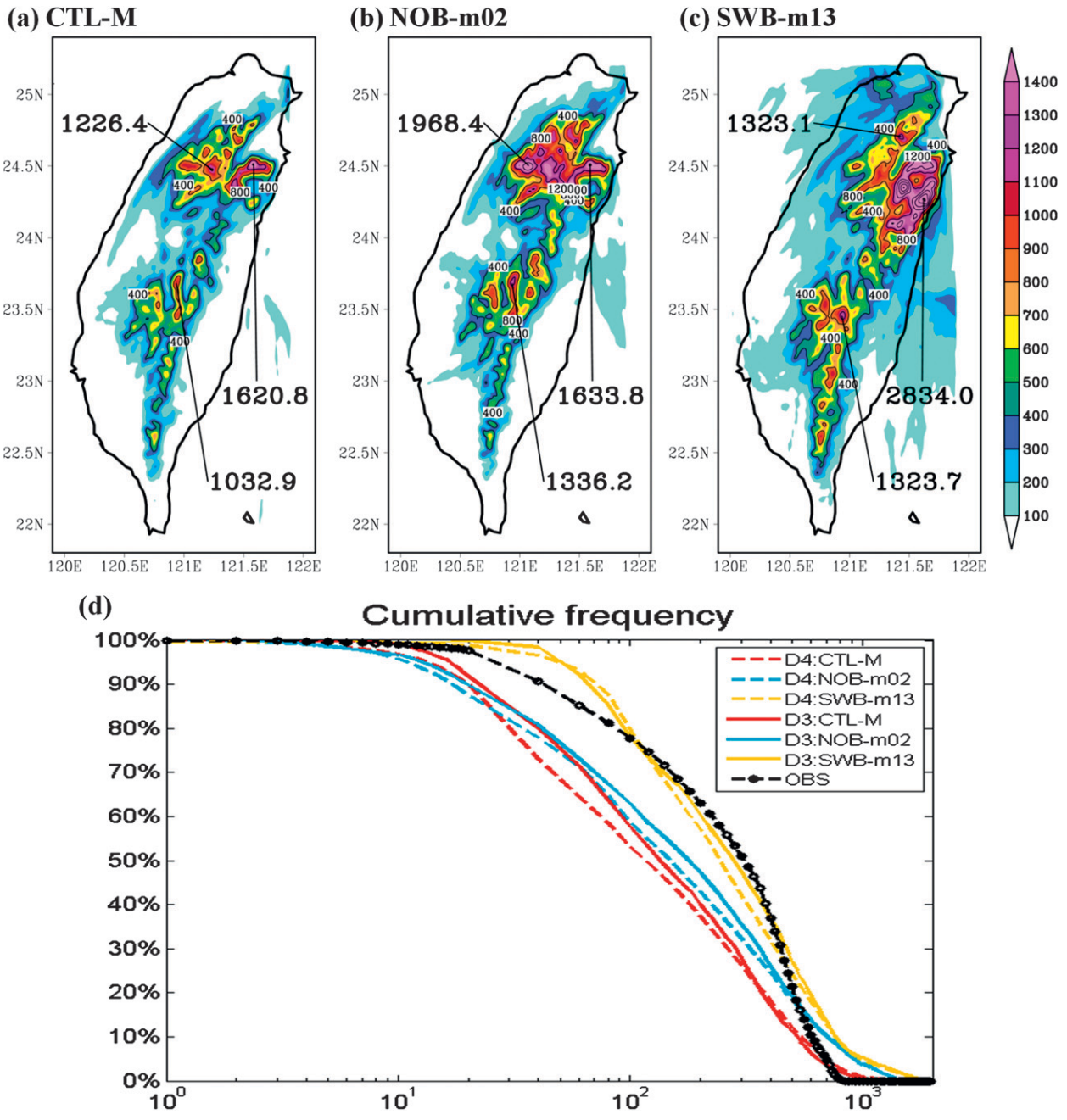

FIG. 15. The 3-day accumulated rainfall (mm) in D4 from 0000 UTC 12 Sep to 0000 UTC 15 Sep 2008 in (a) CTL-M, (b) NOB-m02, and (c) SWB-m13. (d) As in Fig. 4c, but for D3 in CTL-M (solid red line), NOB-m02 (solid blue line), and SWB-m13 (solid yellow line), and for D4 in CTL-M (dashed red line), NOB-m02 (dashed blue line), and SWB-m13 (dashed yellow line), and the observation calculated from rain gauges in CWB (dashed black line).

not shown) since the 3-day accumulated rainfall has already been overestimated in CTL-M, NOB-m02, and SWB-m13 in D3. In the CT area where the maximum accumulated rainfall is underestimated in these three simulations in D3, the ETS at rainfall thresholds between 800 and 900 mm becomes higher in D4 than in D3 (figure not shown), indicating that the higher-resolution simulation helps increase the rainfall amount, which is closer to the observation in CT.

Figure 16 shows that only a small difference in the accumulated rainfall between D4 and D3 is found in the plain area. The areas with increased amount of

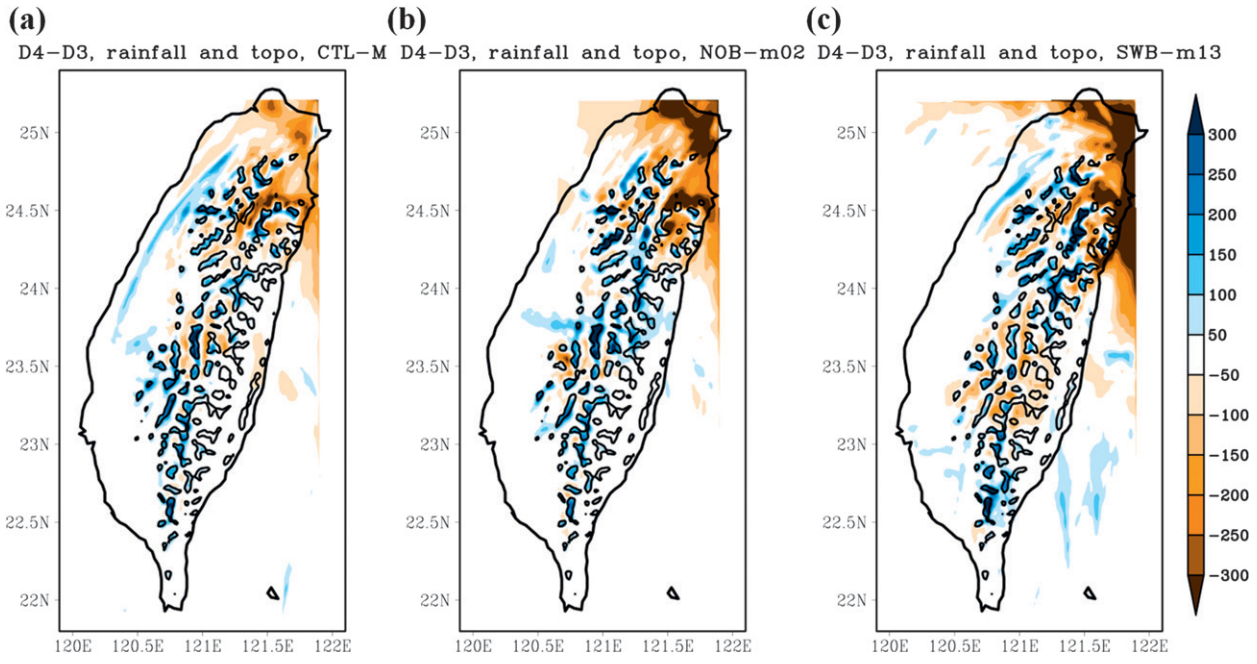

FIG. 16. The difference of the 3-day accumulated rainfall (mm) between D4 and D3 in (a) CTL-M, (b) NOB-m02, and (c) SWB-m13 from 0000 UTC 12 Sep to 0000 UTC 15 Sep 2008. The black contour indicates the difference in terrain height between D4 and D3 is larger than 200 m.

accumulated rainfall are generally collocated with those with increased terrain height in D4. In other words, the significant increase of accumulated rainfall from the higher-resolution simulation mostly occurs over the mountain area (i.e., along CMR), where originally larger accumulated rainfall amount has been measured. However, the mountain area with increased accumulated rainfall covers only a relatively small area percentage (Fig. 16). Thus, the improved resolution does not significantly change the cumulative frequency of the total rainfall.

To better understand why the rainfall amount from the higher-resolution simulation increases, the cross section of the difference in relative humidity and vertical wind between D4 and D3 along 23.5°N in NOB-m02 at the landfall time is demonstrated (Fig. 17). Note that the simulated tracks and TC intensities in the run with higher resolution are surely different from those in the run with lower resolution, thus likely leading to the rainfall differences. However, in order to save computation costs, the fourth nested domain (D4) is designed to be quite small, only covering the area around Taiwan. Therefore, during the simulation time, the center and the structure of storms may not be completely identified in D4 in the ensemble members. The focus of the run with higher resolution is the impact of the Taiwan topography on the rainfall simulation. On the windward side (i.e., the western slope of the mountain as indicated in Fig. 12e), the increase in vertical velocity is generally observed over higher mountains in D4 (Fig. 17) while the major difference in relative humidity is shown to be located at the west of the mountain above 500 hPa and on the lee side. This suggests that the updraft motion (orographic lifting) is enhanced by the better-resolved topography in the higher-resolution simulation, thus leading to the increased rainfall over the mountain area.

4. Summary

Typhoon Sinlaku (2008) produced heavy rainfall over the mountain area of Taiwan, with the maximum 3-day accumulated rainfall measuring about 1211 mm near Hsinchu from 0000 UTC 12 September to 0000 UTC 15 September 2008. The goal of this paper is to explore the impact of different track clusters on the rainfall amounts and distribution in the ensemble simulations. In particular, in this study, the distinct pattern of cumulative frequencies in 28 ensemble members is identified with three types of track clusters [the southwest-biased group (SWB), the no-biased group (NOB), and the northeast-biased group (NEB) with respect to the best track]. In addition, assimilating valuable observation data during T-PARC based on the EnKF data assimilation in WRF assists in improving the initial condition for examining the predictability of the rainfall associated with Sinlaku through the 96-h ensemble simulation with 28 members initialized at 1200 UTC 11 September 2008.

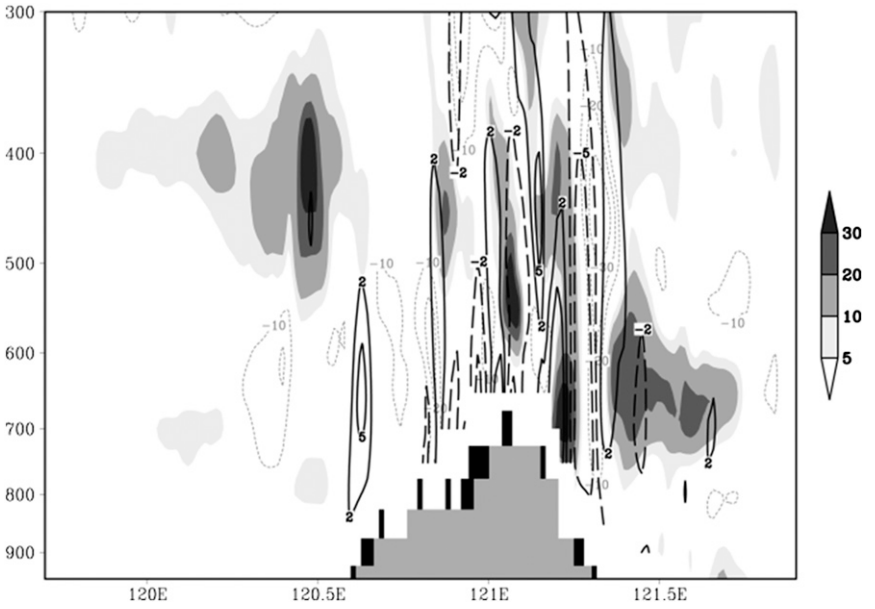

FIG. 17. The cross section of the difference in relative humidity (positive values are shaded and negative values are plotted by dotted gray contours with intervals of 10%) and vertical wind (absolute values larger than 2 m s^{-1} are plotted with black contours) between D4 and D3 along 23.5°N in NOB-m02 at the landfall time. The black and gray areas indicate the topography in D4 and D3, respectively. The vertical pressure coordinate is in logarithmic scale.

The track in the simulation that is integrated from the ensemble mean (CTL-M) is generally consistent with the best track (with the 72-h track forecast error of 95 km) whereas there is a wide spread of tracks among the 28 members. The MSLP averaged by 28 members shows good agreement with the CTL-M simulation. However, the initial storm intensity has a weak bias of about 20 hPa in all ensemble members and the weakening rate during landfall is slightly slower as compared to the best-track analysis. The comparison of 3-day accumulated rainfall indicates that the simulation in CTL-M moderately underestimates the local maximum rainfall amount over the mountain area near Chiayi by about 30% although it marginally captures the overall rainfall pattern in northern and central Taiwan. A quantitative comparison based on the ETS calculated in two identified areas [northern Taiwan (NT) and central Taiwan (CT)] with heavy rainfall signal is conducted to evaluate the rainfall forecast skill. The cumulative frequencies in SWB are closer to the observation as compared to those associated with the other two groups and the ensemble mean of SWB has the highest ETS in CT. The better agreement between SWB and the observation in terms of cumulative frequencies is in part due to the southwestward track bias, which incidentally offsets the undersimulation of rainfall associated with the limitation of model resolution. Nevertheless, SWB produces more rainfall in northeastern Taiwan and also has the largest standard deviation of accumulated rainfall. In NT, the simulation in NOB-m02 has the highest ETS at rainfall thresholds between 300 and 800 mm, followed by CTL-M and the ensemble mean of NOB, indicating that NOB produces more consistent rainfall distribution in northern Taiwan. The simulation in NEB cannot reasonably represent the distribution and amount of accumulated rainfall (with the lowest ETS of nearly zero) since the members have large northeastward track bias and do not make landfall in Taiwan.

A comparison between NOB-m02 and SWB-m13 is conducted in terms of the rainfall distribution from 12 h before landfall to 12 h after landfall. The maximum 6-h accumulated rainfall signal in northern Taiwan (along 24.5°N) in NOB-m02 shifts from the mountain area near Yilan (i.e., the eastern slope of CMR) before landfall to that near Hsinchu (i.e., the western slope) after landfall. In contrast, the major rainfall signal remains in northeastern Taiwan in SWB-m13 during landfall, which is not consistent with the observed pattern, thus leading to the degraded performance with a negative ETS in NT during the 6 h after landfall. The analysis of moisture and wind fields indicates that such distinct difference in rainfall distribution between NOB-m02 and SWB-m13 is mainly attributed to the variation of windward locations, caused by the vortex-scale interactions between the topography and the TCs with different tracks in the ensemble members. However, the impact of environmental moisture field

and storm translation speed on the rainfall distribution differences appears insignificant in the simulation.

The sensitivity experiment in which the horizontal resolution is increased from 5 km in the third domain (D3) to 1.67 km in the fourth nested domain (D4) shows that the maximum accumulated rainfall amount increases with the improved resolution, and that the rainfall amount in central Taiwan in CTL-M is close to that in the observation. In addition, the increase in rainfall amount in D4 mostly occurs over the better-resolved topography associated with the higher resolution in D4. The cross section of vertical velocity differences indicates that the better-resolved topography in D4 results in the enhancement of orographic lifting, thus leading to the increased rainfall accumulation over the mountain area. Nevertheless, the cumulative frequency is not markedly modified by increasing the resolution, since the mountain area with significantly increased accumulated rainfall from the higher-resolution simulation is relatively small, while only limited difference in accumulated rainfall is found in the plain area.

In all, forecasting typhoon-induced rainfall near Taiwan has long been a challenging task because of the complex interaction between typhoon circulation and the topography of Taiwan. For typhoons making landfall in Taiwan, the track often plays a crucial role in the rainfall simulation. Taking advantage of ensemble simulations, this study highlights that the uncertainties in rainfall patterns and amounts can be assessed from ensemble track variations. In addition to the track uncertainties, other factors such as model errors associated with the microphysical and convectional parameterization may also need to be explored. The ensemble simulation that adequately considers those uncertainties and errors can further advance our understanding of heavy rainfall associated with TCs and assist in improving quantitative precipitation forecasting.

Acknowledgments. This work is supported by the National Science Council of Taiwan through Grant NSC 100-2119-M-002-009-MY3 and the Office of Naval Research through Grant N00014-10-1-0725. Valuable comments from Altug Aksoy and an anonymous reviewer that helped improve the quality of the manuscript are highly appreciated.

REFERENCES

Aksoy, A., D. C. Dowell, and C. Snyder, 2009: A multicase comparative assessment of the ensemble Kalman filter for assimilation of radar observations. Part I: Storm-scale analyses. *Mon. Wea. Rev.,* **137,** 1805–1824.

——, ——, and ——, 2010: A multicase comparative assessment of the ensemble Kalman filter for assimilation of radar observations. Part II: Short-range ensemble forecasts. *Mon. Wea. Rev.,* **138,** 1273–1292.

——, S. D. Aberson, T. Vukicevic, K. J. Sellwood, S. Lorsolo, and X. Zhang, 2013: Assimilation of high-resolution tropical cyclone observations with an ensemble Kalman filter using NOAA/AOML/HRD's HEDAS: Evaluation of the 2008–2011 vortex-scale analyses. *Mon. Wea. Rev.,* **141,** 1842–1865.

Atallah, E. H., and L. F. Bosart, 2003: The extratropical transition and precipitation distribution of Hurricane Floyd (1999). *Mon. Wea. Rev.,* **131,** 1063–1081.

Black, T. L., 1994: The new NMC mesoscale Eta model: Description and forecast examples. *Wea. Forecasting,* **9,** 265–278.

Buizza, R., and T. N. Palmer, 1998: Impact of ensemble size on ensemble prediction. *Mon. Wea. Rev.,* **126,** 2503–2518.

Chien, F.-C., Y.-H. Kuo, and M.-J. Yang, 2002: Precipitation forecast of MM5 in the Taiwan area during the 1998 mei-yu season. *Wea. Forecasting,* **17,** 739–754.

Chou, K.-H., and C.-C. Wu, 2008: Typhoon initialization in a mesoscale model—Combination of the bogused vortex and the dropwindsonde data in DOTSTAR. *Mon. Wea. Rev.,* **136,** 865–879.

——, ——, P.-H. Lin, S. D. Aberson, M. Weissmann, F. Harnisch, and T. Nakazawa, 2011: The impact of dropwindsonde observations on typhoon track forecasts in DOTSTAR and T-PARC. *Mon. Wea. Rev.,* **139,** 1728–1743.

Corbosiero, K. L., and J. Molinari, 2002: The effects of vertical wind shear on the distribution of convection in tropical cyclones. *Mon. Wea. Rev.,* **130,** 2110–2123.

Dudhia, J., 1989: Numerical study of convection observed during the Winter Monsoon Experiment using a mesoscale two-dimensional model. *J. Atmos. Sci.,* **46,** 3077–3107.

Elsberry, R. L., and P. A. Harr, 2008: Tropical cyclone structure (TCS08) field experiment science basis, observational platforms, and strategy. *Asia-Pac. J. Atmos. Sci.,* **44,** 209–231.

Evensen, G., 1994: Sequential data assimilation with a nonlinear quasi-geostrophic model using Monte Carlo methods to forecast error statistics. *J. Geophys. Res.,* **99** (C5), 10 143–10 162.

Franklin, J. L., cited 2012: National Hurricane Center forecast verification report. [Available online at http://www.nhc.noaa.gov/verification.]

Goerss, J. S., 2000: Tropical cyclone track forecasts using an ensemble of dynamical models. *Mon. Wea. Rev.,* **128,** 1187–1193.

Grell, G. A., and D. Dévényi, 2002: A generalized approach to parameterizing convection combining ensemble and data assimilation techniques. *Geophys. Res. Lett.,* **29,** 1693, doi:10.1029/2002GL015311.

Hong, S. Y., and J.-O. J. Lim, 2006: The WRF Single-Moment 6-Class Microphysics Scheme (WSM6). *J. Korean Meteor. Soc.,* **42,** 129–151.

——, J. Dudhia, and S. H. Chen, 2004: A revised approach to ice microphysical processes for the bulk parameterization of clouds and precipitation. *Mon. Wea. Rev.,* **132,** 103–120.

——, Y. Noh, and J. Dudhia, 2006: A new vertical diffusion package with an explicit treatment of entrainment processes. *Mon. Wea. Rev.,* **134,** 2318–2341.

Huang, Y.-H., M. T. Montgomery, and C.-C. Wu, 2012: Concentric eyewall formation in Typhoon Sinlaku (2008). Part II: Axisymmetric dynamical processes. *J. Atmos. Sci.,* **69,** 662–674.

Kurihara, Y., M. A. Bender, and R. J. Ross, 1993: An initialization scheme of hurricane models by vortex specification. *Mon. Wea. Rev.,* **121,** 2030–2045.

——, ——, R. E. Tuleya, and R. J. Ross, 1995: Improvements in the GFDL hurricane prediction system. *Mon. Wea. Rev.,* **123,** 2791–2801.

Lin, Y.-L., S. Chiao, T.-A. Wang, M. L. Kaplan, and R. P. Weglarz, 2001: Some common ingredients for heavy orographic rainfall. *Wea. Forecasting,* **16,** 633–660.

Lu, K.-C., 2008: Report on Typhoon 0813 (Sinlaku) of 2008 (in Chinese with an English abstract). Weather Forecast Center, Central Weather Bureau, 23 pp.

Marchok, T., R. Rogers, and R. Tuleya, 2007: Validation schemes for tropical cyclone quantitative precipitation forecasts: Evaluation of operational models for U.S. landfalling cases. *Wea. Forecasting,* **22,** 726–746.

Martin, J. D., 1988: Tropical cyclone observation and forecasting with and without aircraft reconnaissance. Department of Atmospheric Sciences Paper 428, Colorado State University, Fort Collins, CO, 114 pp.

Meng, Z., and F. Zhang, 2007: Tests of an ensemble Kalman filter for mesoscale and regional-scale data assimilation. Part II: Imperfect model experiments. *Mon. Wea. Rev.,* **135,** 1403–1423.

Mlawer, E. J., S. J. Taubman, P. D. Brown, M. J. Iacono, and S. A. Clough, 1997: Radiative transfer for inhomogeneous atmospheres: RRTM, a validated correlated-*k* model for the longwave. *J. Geophys. Res.,* **102** (D14), 16 663–16 682.

Naval Research Laboratory, 1999: Tropical cyclone forecasters' reference guide. [Available online at http://www.nrlmry.navy.mil/~chu/.]

Pu, Z.-X., and S. A. Braun, 2001: Evaluation of bogus vortex techniques with four-dimensional variational data assimilation. *Mon. Wea. Rev.,* **129,** 2023–2039.

Rappaport, E. N., and Coauthors, 2009: Advances and challenges at the National Hurricane Center. *Wea. Forecasting,* **24,** 395–419.

Rogers, R., S. Chen, J. Tenerelli, and H. Willoughby, 2003: A numerical study of the impact of vertical shear on the distribution of rainfall in Hurricane Bonnie (1998). *Mon. Wea. Rev.,* **131,** 1577–1599.

Schaefer, J. T., 1990: The critical success index as an indicator of warning skill. *Wea. Forecasting,* **5,** 570–575.

Snyder, C., and F. Zhang, 2003: Assimilation of simulated Doppler radar observations with an ensemble Kalman filter. *Mon. Wea. Rev.,* **131,** 1663–1677.

Sung, S.-L., C.-C. Wu, and S. S. Chen, 2010: Impact of the upper-ocean thermal structure on typhoon intensity change in a coupled atmosphere–ocean model. Preprints, *29th Conf. on Hurricanes and Tropical Meteorology,* Tucson, AZ, Amer. Meteor. Soc., 12A.5. [Available online at https://ams.confex.com/ams/29Hurricanes/techprogram/paper_168108.htm.]

Szunyogh, I., E. J. Kostelich, G. Gyarmati, E. Kalnay, B. R. Hunt, E. Ott, E. Satterfield, and J. A. Yorke, 2008: A local ensemble transform Kalman filter data assimilation system for the NCEP global model. *Tellus,* **60A,** 113–130.

Tao, W. K., and Coauthors, 2011: High-resolution numerical simulation of the extreme rainfall associated with Typhoon Morakot. Part I: Comparing the impact of microphysics and PBL parameterizations with observations. *Terr. Atmos. Oceanic Sci.,* **22,** 673–696.

Torn, R. D., and G. J. Hakim, 2008: Performance characteristics of a pseudo-operational ensemble Kalman filter. *Mon. Wea. Rev.,* **136,** 3947–3963.

——, and ——, 2009: Ensemble data assimilation applied to RAINEX observations of Hurricane Katrina (2005). *Mon. Wea. Rev.,* **137,** 2817–2829.

Wang, Y., and C.-C. Wu, 2004: Current understanding of tropical cyclone structure and intensity changes—A review. *Meteor. Atmos. Phys.,* **87,** 257–278.

Weissmann, M., and Coauthors, 2011: The influence of dropsondes on typhoon track and midlatitude forecasts. *Mon. Wea. Rev.,* **139,** 908–920.

Whitaker, J. S., and T. M. Hamill, 2002: Ensemble data assimilation without perturbed observations. *Mon. Wea. Rev.,* **130,** 1913–1924.

——, ——, X. Wei, Y. Song, and Z. Toth, 2008: Ensemble data assimilation with the NCEP Global Forecast System. *Mon. Wea. Rev.,* **136,** 463–482.

Wu, C.-C., 2013: Typhoon Morakot: Key findings from the journal *TAO* for improving prediction of extreme rains at landfall. *Bull. Amer. Meteor. Soc.,* **94,** 155–160.

——, and Y.-H. Kuo, 1999: Typhoons affecting Taiwan: Current understanding and future challenges. *Bull. Amer. Meteor. Soc.,* **80,** 67–80.

——, T.-H. Yen, Y.-H. Kuo, and W. Wang, 2002: Rainfall simulation associated with Typhoon Herb (1996) near Taiwan. Part I: The topographic effect. *Wea. Forecasting,* **17,** 1001–1015.

——, K.-H. Chou, Y. Wang, and Y.-H. Kuo, 2006: Tropical cyclone initialization and prediction based on four-dimensional variational data assimilation. *J. Atmos. Sci.,* **63,** 2383–2395.

——, ——, P.-H. Lin, S. D. Aberson, M. S. Peng, and T. Nakazawa, 2007: The impact of dropwindsonde data on typhoon track forecasts in DOTSTAR. *Wea. Forecasting,* **22,** 1157–1176.

——, G.-Y. Lien, J.-H. Chen, and F. Zhang, 2010: Assimilation of tropical cyclone track and structure based on the ensemble Kalman filter (EnKF). *J. Atmos. Sci.,* **67,** 3806–3822.

——, S.-G. Chen, C.-C. Yang, P.-H. Lin, and S. D. Aberson, 2012a: Potential vorticity diagnosis of the factors affecting the track of Typhoon Sinlaku (2008) and the impact from dropwindsonde data during T-PARC. *Mon. Wea. Rev.,* **140,** 2670–2688.

——, Y.-H. Huang, and G.-Y. Lien, 2012b: Concentric eyewall formation in Typhoon Sinlaku (2008). Part I: Assimilation of T-PARC data based on the ensemble Kalman filter (EnKF). *Mon. Wea. Rev.,* **140,** 506–527.

Yang, M.-J., D.-L. Zhang, and H.-L. Huang, 2008: A modeling study of Typhoon Nari (2001) at landfall. Part I: Topographic effects. *J. Atmos. Sci.,* **65,** 3095–3115.

Yen, T.-H., C.-C. Wu, and G.-Y. Lien, 2011: Rainfall simulations of Typhoon Morakot with controlled translation speed based on EnKF data assimilation. *Terr. Atmos. Oceanic Sci.,* **22,** 647–660.

Zhang, F., Z. Meng, and A. Aksoy, 2006: Tests of an ensemble Kalman filter for mesoscale and regional-scale data assimilation. Part I: Perfect model experiments. *Mon. Wea. Rev.,* **134,** 722–736.

——, Y. Weng, J. A. Sippel, Z. Meng, and C. H. Bishop, 2009: Cloud-resolving hurricane initialization and prediction through assimilation of Doppler radar observations with an ensemble Kalman filter: Humberto (2007). *Mon. Wea. Rev.,* **137,** 2105–2125.

——, ——, Y.-H. Kuo, J. S. Whitaker, and B. Xie, 2010: Predicting Typhoon Morakot's catastrophic rainfall with a convection-permitting mesoscale ensemble system. *Wea. Forecasting,* **25,** 1816–1825.

Zhu, T., and D.-L. Zhang, 2006: Numerical simulation of Hurricane Bonnie (1998). Part II: Sensitivity to varying cloud microphysical processes. *J. Atmos. Sci.,* **63,** 109–126.

Zou, X., and Q. Xiao, 2000: Studies on the initialization and simulation of a mature hurricane using a variational bogus data assimilation scheme. *J. Atmos. Sci.,* **57,** 836–860.